Sheffield Hallam University

Multiaxial fatigue assessment of ColdArc®-welded aluminium-to-steel hybrid joints

NG, Chin Tze <http://orcid.org/0000-0002-0663-4798> and SUSMEL, Luca <http://orcid.org/0000-0001-7753-9176>

Available from Sheffield Hallam University Research Archive (SHURA) at:

https://shura.shu.ac.uk/37058/

This document is the Accepted Version [AM]

Citation:

NG, Chin Tze and SUSMEL, Luca (2026). Multiaxial fatigue assessment of ColdArc®-welded aluminium-to-steel hybrid joints. International Journal of Fatigue: 109606. [Article]

Copyright and re-use policy

See http://shura.shu.ac.uk/information.html

Sheffield Hallam University Research Archive
http://shura.shu.ac.uk

Multiaxial Fatigue Assessment of ColdArc®-Welded Aluminium-to-Steel Hybrid Joints

Chin Tze Ng[1], Luca Susmel[2]

[1]School of Mechanical, Aerospace and Civil Engineering, The University of Sheffield, Mappin Street, Sheffield S1 3JD, UK

[2]Materials and Engineering Research Institute, Sheffield Hallam University, Harmer Building, Sheffield, S1 1WB, UK

Corresponding author: Professor **Luca Susmel**, Materials and Engineering Research Institute, Sheffield Hallam University, Harmer Building, Sheffield, S1 1WB, UK, email: l.susmel@shu.ac.uk

ABSTRACT

This study investigates the multiaxial fatigue behaviour of coldArc®-welded AA6082-T6 aluminium-to-S235 steel tubular joints and evaluates the effectiveness of established fatigue criteria when combined with different stress-analysis approaches. Fatigue tests were conducted under uniaxial, torsional, proportional, and 90° out-of-phase loading, across stress ratios (R) of –1 and 0.1. All fatigue failures initiated from the aluminium side, confirming aluminium as the fatigue-critical region in this configuration. Mean stress effects were modest, and non-proportional loading did not significantly reduce fatigue life, supporting the use of simplified multiaxial fatigue models for this joint configuration. Increasing shear stress contribution consistently reduced fatigue strength, highlighting the influence of biaxiality ratio. Three stress analysis approaches were examined for fatigue life estimation: the Nominal Stress method, the Fictitious Notch Radius approach with a reference fictitious radius of 0.05 mm, and the Theory of Critical Distances - Point Method (TCD-PM). These were used with the International Institute of Welding (IIW), Eurocode 9 (EC9), and the Modified Wöhler Curve Method (MWCM) criteria and benchmarked against experimental dataset. The results show that IIW and EC9, when paired with nominal stresses, provided safe and consistent predictions, local stress-based approaches improved accuracy, and the TCD-PM delivered reliable estimations without requiring notch-radius assumptions. Overall, the combined experimental evidence and comparative estimated fatigue life assessments clarify the suitability and practical selection of multiaxial fatigue assessment methods for aluminium-to-steel welded joints in engineering applications.

Keywords: Multiaxial fatigue, hybrid welded joints, aluminium-steel, critical plane, fatigue life estimation, IIW, stress analysis

NOMENCLATURE

$\Delta\sigma$	Normal stress range
$\Delta\sigma_x$	Normal stress range in x-direction
$\Delta\tau$	Shear stress range
$\Delta\tau_{xy}$	Shear stress range in xy-direction
σ_a	Normal stress amplitude
τ_a	Shear stress amplitude
$\Delta\sigma_{nom}$	Nominal normal stress range
$\Delta\tau_{nom}$	Nominal shear stress range
$\Delta\sigma_{FNR}$	Normal stress range from FNR approach
$\Delta\tau_{FNR}$	Shear stress range from FNR approach
$\Delta\sigma_n$	Normal stress range relative to the critical plane
ρ_w	MWCM multiaxiality stress ratio parameter for welded joints
$\rho_{w,lim}$	Limiting value of the MWCM multiaxiality stress ratio parameter for welded joints
λ	Biaxiality ratio (σ_a/τ_a)
δ	Phase angle for biaxial fatigue loading
$\Delta\sigma_R$	Reference normal stress corresponding to N_R cycles to failure
$\Delta\tau_R$	Reference shear stress corresponding to N_R cycles to failure
$\Delta\sigma_{R,Ps=97.7\%}$	Reference normal stress range at N_{Ref} cycles recalculated for a P_s of 97.7%
$\Delta\tau_{R,Ps=97.7\%}$	Reference shear stress range at N_{Ref} cycles recalculated for a P_s of 97.7%
T_σ	Scatter ratio for normal stress fatigue data
T_τ	Scatter ratio for shear stress fatigue data
R	Stress ratio
k	Negative inverse slope for uniaxial S-N curve
k0	Negative inverse slope for pure torsional S-N curve
K_{ta}	Normal stress concentration factor under uniaxial loading
K_{tt}	Shear stress concentration factor under torsional loading
P_s	Probability of survival
r_{ref}	Fictitious reference notch radius used in the FNR approach
$\Delta\tau_{R,MWCM}$	MWCM reference shear stress range at N_R cycles to failure
$\Delta\sigma_1$	Absolute maximum principal stress range
$\Delta\sigma_{IIW}$	Effective equivalent stress range based on the IIW criterion
$\Delta\sigma_{criterion}$	Effective equivalent stress range defined by respective fatigue criterion
N_f	Experimental number of cycles to failure
$N_{f,e}$	Estimated number of cycles to failure
$N_{f(i)}$	Experimental number of cycles to failure for test i
$N_{f,e(i)}$	Estimated number of cycles to failure for test i
N_{kp}	Number of cycles at the S-N curve knee point
N_{Ref}	Reference number of cycles to failure (2 million cycles)
n	Total number of observations in each test series
P_{NC}	Percentage of non-conservative estimates
P_C	Percentage of conservative estimates
CV_{IIW}	Comparison value
M-D_v	Critical distance for the TCD PM
T_{RMS}	Performance metric to assess accuracy of each fatigue criterion; lower values indicate higher predictive accuracy
RMSLE	Root mean squared logarithmic error
CA	Constant amplitude
EC3	Eurocode 3
EC9	Eurocode 9
FNR	Fictitious Notch Radius
FE	Finite Element
IIW	International Institute of Welding
MP	Maximum Principal Stress Criterion

MWCM	Modified Wöhler Curve Method
NS	Nominal Stress
N-SIF	Notch Stress Intensity Factor
PM	Point Method
TCD	Theory of Critical Distances
WR	Weld Root
WT	Weld Toe
SCFs	Stress Concentration Factors

1. Introduction

The growing demand for lightweight, high-performance, and environmentally sustainable structures has driven increasing interest in hybrid aluminium-to-steel welded joints across automotive, offshore, and civil engineering sectors. These dissimilar joints combine the favourable properties of both materials: aluminium offers low density, corrosion resistance, and recyclability, while steel provides higher strength and load-bearing capacity. Their integration enables structural weight reduction without compromising strength or safety.

Despite its growing industrial application, there is still a lack of available experimental data and validated fatigue assessment approaches for aluminium-to-steel welded joints, particularly under multiaxial loading. Most fatigue assessment methodologies have been developed independently for either homogeneous steel or aluminium welded joints [1–5]. While numerous studies have characterised the fatigue behaviour of these welded joints under both uniaxial and multiaxial loading [6–10], the direct application of these models to hybrid aluminium-to-steel welded joints has not yet been systematically evaluated.

Examination of the state-of-the-art reveals that existing investigations on hybrid aluminium-to-steel welded joints have largely been limited to uniaxial loading conditions [11–13]. While informative, uniaxial fatigue data do not reflect the multiaxial stress states commonly encountered in service, limiting their applicability in realistic design scenarios. Furthermore, no prior study has systematically investigated the multiaxial fatigue behaviour of thin coldArc®[1]-welded aluminium-to-steel joints.

To address these knowledge gaps, this study provides a comprehensive experimental characterisation of coldArc®-welded AA6082-T6 aluminium-to-S235 steel tubular joints under constant amplitude multiaxial loading. Fatigue tests were conducted under uniaxial, pure torsional, in-phase, and 90° out-of-phase loading conditions. The experimental programme establishes the fatigue-critical regions, identifies failure mechanisms, and develops characterised S–N curves using both nominal and local stress definitions. These datasets form the basis for evaluating multiaxial fatigue criteria.

[1] ColdArc® is a registered trademark of EWM AG.

Building on this foundation, three stress analysis approaches: Nominal Stress (NS), Fictitious Notch Radius (FNR), and the Theory of Critical Distances- Point Method (TCD PM) are examined. Each approach is used in combination with established multiaxial fatigue criteria - the International Institute of Welding (IIW), maximum principal stress (MP) criterion, and the Modified Wöhler Curve Method (MWCM) - to assess their predictive performance across proportional and non-proportional loading paths.

The aim is to establish a practical fatigue assessment procedure for hybrid aluminium-to-steel welded joints. By comparing the accuracy, conservatism, and feasibility of each method, this study identifies reliable modelling strategies for engineering application and offers insight into the trade-offs between modelling complexity and predictive performance. The outcomes support the development of reliable multiaxial fatigue-life estimation methods for hybrid welded joints, enabling safer and more efficient design in engineering practice.

2. Experimental Overview

Hybrid tubular specimens were manufactured by circumferentially joining AA6082-T6 aluminium to zinc-coated S235 steel using the EWM coldArc® welding process with AWS A5.10 ER4043 filler material. The welded joints comprised 1 mm thick aluminium and steel hollow tubes joined with a 15 mm overlap, as illustrated in Fig. 1. The coldArc® process was selected for its controlled low heat input, which minimises the formation of brittle intermetallic compounds at the dissimilar metal interface. Full details on welding parameters, material properties, and specimen preparation are reported in the authors' previous publication [14].

Fatigue testing was conducted on the as-welded joints under constant amplitude (CA) sinusoidal loading at a frequency of 10 Hz. Four loading configurations were applied: uniaxial, pure torsion, in-phase, and 90° out-of-phase fatigue loading. To investigate the effects multiaxiality on the critical plane and fatigue life, biaxiality ratios ($\lambda=\sigma_a/\tau_a$) of 1 and $\sqrt{3}$ were used. Additionally, two stress ratios ($R=\sigma_{min}/\sigma_{max}$ or $R=\tau_{min}/\tau_{max}$) of -1 and 0.1 were employed to assess mean stress effects. The corresponding loading paths are shown in Fig. 2, covering both proportional and non-proportional stress conditions.

Stress amplitudes were selected to target the medium to high cycle fatigue regime, with failure lives ranging from 10^3 to 2 million cycles. Specimens that reached the runout threshold of 2 million cycles were subsequently retested at higher stress amplitudes. Fatigue failure was defined as a 10% reduction in stiffness, typically associated with surface crack formation between 10 to 20 mm in length.

This experimental programme produced a comprehensive dataset characterising the multiaxial fatigue behaviour of hybrid aluminium-to-steel welded joints. These results form a crucial foundation for the failure analysis and fatigue characterisation presented in this study, which in turn support the

development of multiaxial fatigue life estimation framework detailed in a related study. Further details on the experimental setup, test matrix, and specimen design rationale can be found in [14].

3. Failure Mechanisms and Localised Weld Geometry Observations

Detailed observations of crack initiation and local weld geometry were undertaken to support the modelling assumptions used in this study. To investigate crack initiation mechanisms, eight sectioned hybrid specimens comprising four undamaged welded joints and four that had failed during fatigue testing, were examined using a Nikon optical microscope at 5× and 10× magnification. This enabled direct visualisation of weld features and identification of potential crack initiation sites at weld toe and root. A depiction of these observed weld features, including optical micrographs with annotated insets, is presented in Fig. 3.

Consistent with previous findings [14], crack initiation consistently occurred at the aluminium weld toe and the aluminium-side weld root (WR2), with no initiation observed at the steel weld toe, likely due to the higher fatigue strength of the steel side. Sectioning of specimens followed by optical microscopy revealed two weld root features within the aluminium region (WR1 and WR2), clarifying the weld root geometry that is not visible from the external surface. This observation further supports the selection of both the aluminium weld toe and WR2 as fatigue-critical sites for localised stress analysis. Due to the thin-walled geometry of the tubular hybrid joints, distinguishing between failures at the weld toe and WR2 was challenging. In some cases, observations suggested that cracks may have initiated at both sites simultaneously with crack growth converging along a common failure path. As such, the aluminium weld toe and WR2 were grouped as a single critical initiation failure category.

In the FNR approach adopted in this study, a reference radius of r = 0.05 mm was applied at the weld toe and root in accordance with the IIW and Sonsino's recommendations for thin welded joints below 5 mm [5,15,16]. Crack-orientation analysis further informed the selection of suitable multiaxial fatigue criteria. Fig. 4 shows a representative specimen used to determine initiation and propagation angles. Tested under in-phase biaxial loading, this specimen retained a clearly visible crack along the aluminium toe/root region, allowing the initiation angle to be measured over the first 1–2 mm of growth before transitioning into the propagation direction. Although the visible crack extends slightly beyond the strict initiation scale, its geometry remained sufficiently intact to illustrate the measurement procedure. Consistent with previous findings in [14], the crack initiated along a direction close to the plane of maximum shear stress and subsequently propagated toward the plane of maximum normal stress. This stage-dependent crack trajectory reinforces the need for multiaxial fatigue criteria that capture both shear and normal stress effects.

Together, these findings establish a physically grounded basis for defining stress extraction paths in FEA and establishing appropriate modelling assumptions for the subsequent multiaxial fatigue-life estimations.

4. Fatigue Behaviour and S–N Curve Evaluation

This section presents the fatigue behaviour of coldArc®-welded thin hybrid aluminium-to-steel tubular joints under uniaxial, pure torsional, and multiaxial loading conditions. All stress ranges are expressed in terms of nominal stresses evaluated from the aluminium tube cross-section adjacent to the weld, given that fatigue consistently initiated in the aluminium region. The tubular configuration is essentially coaxial, so any load-path eccentricity is expected to be small. Therefore, nominal stresses were defined directly on the aluminium section, while local effects associated with weld geometry and any secondary bending are captured within the localised stress-based approaches.

S–N curves were obtained by least-squares linear regression in log-log space, treating log N_f as the dependent variable and minimising the scatter in the log N-direction, consistent with the IIW recommendations. The resulting regression line defines the 50% survival curve. Assuming a lognormal distribution of fatigue life, the scatter was quantified by the standard deviation of the log N residuals, and probability of survival (P_s) scatter bands of 2.3% and 97.7% were constructed by shifting the P_s of 50% curve in the log N direction using a one-sided statistical tolerance factor corresponding to a confidence level of 95%, which depends on the available sample size. No knee point was fitted, and a single slope is used over the investigated life range. Figs 5a and 5b show the S-N curves for uniaxial and torsional loading conditions, respectively, based solely on fully reversed (R=-1) fatigue data. Key parameters such as the reference fatigue strength at P_s of 50%, the negative inverse slope (k), and scatter ratios (T_σ and T_τ) as derived from Eq. 1 were extracted from the regression analysis and summarised alongside the figures.

$$T_\sigma = \frac{\Delta\sigma_{R,P_S=2.3\%}}{\Delta\sigma_{R,P_S=97.7\%}} \quad (1)$$

To evaluate the influence of mean stress, additional tests were performed at R=0.1 for both uniaxial and torsional loading. These data were overlaid onto the previously derived R=-1 scatter bands as shown in Figs 5c and 5d. The S–N data for both R-ratios were re-evaluated using a common slope to assess the mean stress sensitivity. The resulting parallel S–N curves showed a reduction in fatigue strength at R = 0.1 relative to R = –1, with decreases of approximately 20% under uniaxial loading and 15% under pure torsion at 2×10^6 cycles. This confirms the presence of a moderate mean stress effect. This trend is consistent with the high tensile residual stresses inherently present in as-welded joints, which raise the local effective stress ratio toward positive values even when the nominal loading is fully reversed

[17,18]. As a result, the difference between R = -1 and R = 0.1 conditions becomes less pronounced compared with stress-relieved welded joints but is not absent.

It is worth noting that the R = 0.1 dataset comprises only four specimens for uniaxial and pure torsional case, respectively. Therefore, the calculated mean stress sensitivity values should be interpreted as indicative trends rather than statistically definitive. Given this limited sample size for R = 0.1 data, the parallel-slope representation provides a reasonable and transparent way to illustrate the trend without overstating its accuracy. For the present as-welded joints, the R = 0.1 data indicate a noticeable reduction in fatigue strength relative to R = -1. However, the limited range of stress ratios in the present dataset does not support generalisation to higher R values. Accordingly, both the R = -1 and R = 0.1 datasets were retained when characterising fatigue parameters for the subsequent stress analysis approaches.

5. Effect of Loading Proportionality and Biaxiality on Multiaxial Fatigue Behaviour

In addition to mean stress effects, two important parameters influencing multiaxial fatigue behaviour are loading proportionality, defined by the phase relationship between normal and shear stresses, and the biaxiality ratio (λ), which quantifies the relative contribution of axial to shear loading. This section examines how variations in these parameters affect the fatigue performance of coldArc®-welded hybrid aluminium-to-steel tubular joints.

To assess the influence of loading proportionality, S–N curves were generated for in-phase and 90° out-of-phase multiaxial loading conditions. Fig. 6 shows the S-N curves at a P_s of 50%, while the full experimental dataset (nominal stress-based) under CA is summarised in Tab. 1.

The results show no significant reduction in fatigue strength under out-of-phase loading when compared to in-phase loading, irrespective of λ. This finding contrasts with typical behaviour in conventional welded steel joints, where non-proportionality is typically associated with increased damage accumulation. For welded aluminium joints, however, Sonsino reported minimal sensitivity to non-proportional loading [19,20]. The present results are consistent with these observations, suggesting that the aluminium region in these hybrid joints is relatively insensitive to non-proportional loading effects. Consequently, simplified fatigue models that do not explicitly account for loading proportionality may be sufficient for such hybrid aluminium-to-steel welded joints.

The influence of biaxiality ratio was also explored by comparing tests conducted at λ of √3 and 1. A reduction in λ increases the contribution of shear stress relative to normal stress, which resulted in a systematic reduction in fatigue strength across both load paths. This trend is consistent with the observation that the fatigue strength under shear is lower than under normal loading. Therefore, when the shear component becomes more dominant, it promotes earlier crack initiation and accelerates fatigue

damage, aligning with observations in Section 3, where cracks initiated along planes dominated by shear stress. As shear-driven mechanisms become more prominent at lower biaxiality ratios, the need for multiaxial fatigue criteria that incorporate both shear and normal stress components becomes evident.

In summary, the fatigue strength of coldArc®-welded hybrid joints exhibited negligible sensitivity to non-proportional loading but a clear reduction in fatigue strength with increasing shear contribution. These findings emphasise the importance of accounting for multiaxial stress interaction and support the use of fatigue models capable of capturing both shear and normal stress effects.

6. Fatigue Strength Characterisation and Stress Analysis Overview

This section summarises the fatigue strength parameters derived for coldArc®-welded aluminium-to-steel tubular joints using three stress analysis approaches: NS, FNR, and the TCD PM [1,2,5,16,21]. These methods range from global nominal to localised stress-based approaches and are used to extract the critical stress states at potential crack initiation sites, resulting in different equivalent stress inputs for fatigue life estimation. The resulting experimentally derived S-N curves for the NS and FNR approaches are presented in Fig. 7a-d.

For the NS approach, nominal normal and shear stresses were computed using the aluminium tube's cross-sectional area adjacent to the weld, since all failures consistently initiated on the aluminium side. The nominal area was calculated from the mean outer and inner diameters (44.40 mm and 42.40 mm), as shown in Fig. 1.

The FNR approach accounts for local notch effects by introducing a fictitious radius at the weld toe and root. Following the latest IIW and Sonsino recommendations for thin-walled welded joints ($t < 5$ mm), a reduced fictitious radius of 0.05 mm was adopted [5,15,22]. This value better captures the notch sensitivity of thin-walled structures while maintaining a practical balance between modelling accuracy and computational efficiency [5,15,22].

The TCD PM approach was adopted as an alternative local method and applied in conjunction with the MWCM criterion. In this formulation, weld toes and roots are idealised as sharp notches with zero radius, implemented using the widely adopted sharp-notch TCD-PM framework for welded aluminium and steel joints. TCD can also be applied using finite-radius notch fields; however, this requires a consistent recalibration of the critical distance, M-D_v for the adopted notch idealisation. Such recalibration requires ground butt-welded calibration specimens and uniaxial reference curves, which is an approach not feasible for coldArc® joints because the welding process inherently requires a lapped configuration and cannot produce ground butt-welds for calibration. Accordingly, the sharp-notch formulation was selected as both methodologically appropriate and practically necessary for the present study.

Within the TCD PM framework, fatigue strength is governed by the stress state at a specific material-dependent critical distance, M-D_v, measured from the notch tip along a focus path oriented through the notch bisector. As hybrid coldArc® joints cannot be calibrated directly, established values from the literature for welded aluminium and steel joints are adopted. These values were originally obtained through a two-curve calibration procedure, where a plain (un-notched) fatigue reference curve and a sharp-notch reference curve, derived using Notch Stress Intensity Factors (N-SIFs), are combined to determine a material length scale that links the two regimes. This procedure is described in detail in previous TCD developments for welded joints [6,23–26]. Accordingly, a M-D_v of 0.075 mm is used for aluminium weld toes and roots, and 0.5 mm for the steel weld toe [6,23–26]. These values are considered inherent material properties, independent of geometry or loading complexity.

The experimentally derived fatigue strengths and slopes at P_s of 97.7% for each approach are summarised in Tab. 2. For NS and FNR, these were benchmarked against reference values from EC9 and IIW recommendations. This comparison provides a practical context to assess whether current design classifications offer conservative or representative fatigue strength predictions for coldArc®-welded hybrid joints.

By combining experimentally characterised parameters with established reference values across multiple stress-analysis strategies, this section provides a coherent and physically justified basis for the multiaxial fatigue life assessments.

7. Finite Element Modelling

A 2D axisymmetric linear-elastic finite element model was developed in ANSYS APDL to extract the local stress fields required for the FNR and TCD-PM approaches. PLANE25 harmonic elements were used as they efficiently represent combined axial and torsional loading in tubular welded joints while providing sufficiently accurate elastic peak stresses at weld toes and roots. The model geometry incorporated the experimentally observed weld features together with the reference fictitious radius of 0.05 mm adopted in the FNR approach. The FE model of the weld region together with the representative maximum principal stress contour distributions under a nominal axial and torsional stress range of 1 MPa for the FNR and TCD PM approaches are shown in Figs. 8a and 8b. The aluminium (AA6082-T6) and steel (S235) tubes were modelled as distinct material regions separated by a sharp interface, reflecting the actual discontinuity in elastic modulus (Youngs Modulus, E = 70 GPa, Poisson's ratio, $\nu = 0.33$ for aluminium; E = 210 GPa, $\nu = 0.30$ for steel). As a result, the elevated stresses predicted at the interface reflect the combined effect of geometric discontinuity and elastic modulus mismatch between the two materials.

Local mesh refinement was applied in all fatigue-critical regions. For the FNR formulation, the minimum element size was approximately 0.01 mm, with convergence of the maximum principal stress achieved at ~570 000 elements in total. For the TCD-PM model, which requires evaluating the stress at a critical distance under a sharp-notch assumption, the mesh was refined down to 0.008 mm along the focus path, and stress convergence at the critical distance M-D_v was reached with ~1.7 million elements in total. Linear-elastic material behaviour was assumed throughout, enabling stress superposition for combined axial-torsional loading.

Stresses were extracted at all potential crack-initiation locations on both the aluminium and steel sides. Although the steel weld toe exhibited higher elastic peak stresses due to modulus mismatch, its higher intrinsic fatigue strength would imply that any hypothetical crack path entering the steel region would result in a longer estimated fatigue life. Therefore, across all modelling approaches, the fatigue behaviour was governed by the aluminium weld toe, consistent with the experimental failure mode observations.

The weld-root profile adopted in the FE model - represented by two idealised radii (WR1 and WR2) connected by a smooth transition is a simplification of the actual joint geometry. Alternative plausible root shapes, such as a more pronounced U-shaped corner, would inevitably modify the local stress concentration factors (SCFs) to some extent. However, such variations do not alter the identification of the critical hotspot, which consistently remained at the aluminium side in agreement with the experimental observations.

To quantify the effect of notch-radius idealisation on local stress amplification, the SCFs obtained from the FE analyses for the FNR and TCD-PM approaches are summarised in Tab. 3. The inclusion of the TCD-PM approach, which operates directly on the sharp-notch stress field through a material critical distance, was intended to evaluate the robustness of fatigue life estimations against uncertainties in the assumed root geometry.

Overall, the FE modelling strategy strikes an appropriate balance between geometric realism, computational efficiency, and the accurate resolution of local stress gradients. Despite unavoidable idealisations inherent to welded joint modelling, all stress-analysis methods produced fatigue-life estimates that remained within the experimental scatter, confirming that the adopted modelling approach provides a sufficiently accurate basis for the fatigue assessments carried out in this study.

8. Fundamentals of Multiaxial Fatigue Criteria

This study evaluates three multiaxial fatigue criteria to estimate the fatigue life of thin coldArc®-welded aluminium-to-steel hybrid joints under CA loading: the IIW criterion, the EC9 criterion, and the MWCM. The IIW and EC9 criteria are established in design standards that offer practical procedures

for multiaxial fatigue assessment, while the MWCM represents a critical plane approach developed to capture multiaxial fatigue behaviour.

The IIW criterion is based on Gough-Pollard type interaction equation that combines the applied normal and shear stress ranges into a quadratic form as shown in Eq. 2 [5]:

$$\left(\frac{\Delta\sigma_x}{\Delta\sigma_R}\right)^2 + \left(\frac{\Delta\tau_{xy}}{\Delta\tau_R}\right)^2 \leq CV_{IIW} \quad (2)$$

Based on this interaction equation, the welded joint is deemed safe if the combined stress range does not exceed the design threshold, typically associated with a reference fatigue life of two million cycles. This interaction can also be visualised through standard interaction diagrams, where points falling within the boundary of the interaction curve represents safe estimates whereas points lying beyond the boundary of the interaction curve suggests unsafe estimates [5]. While this interaction equation is inherently suited for binary pass or fail checks, it can be reformulated to enable fatigue life estimation through an equivalent stress expression as expressed in Eq. 3 [27–29].

$$\Delta\sigma_{IIW} = \frac{1}{\sqrt{CV_{IIW}}} \cdot \sqrt{\Delta\sigma_x^2 + \frac{\Delta\sigma_R^2}{\Delta\tau_R^2} \cdot \Delta\tau_{xy}^2} \quad (3)$$

To allow direct comparison of the fatigue life estimates, Eq. 4 is used throughout this study to compute the equivalent stress range for life estimation under the IIW criterion.

On the other hand, the EC9 criterion adopts the maximum principal stress criterion, which is appropriate for aluminium welded joints [2]. Since EC9 does not provide an explicit expression for this quantity, the maximum principal stress range was computed in this study using the standard elastic principal stress formulation commonly employed in multiaxial fatigue analysis [27]. The adopted expression is as defined in Eq. 4.

$$\Delta\sigma_1 = \left(\Delta\sigma_x + \Delta\sigma_y + \sqrt{\left(\Delta\sigma_x - \Delta\sigma_y\right)^2 + 4\Delta\tau_{xy}^2}\right)/2 \quad (4)$$

The MWCM, in contrast, is a critical plane criterion that considers the multiaxiality of loading by identifying the material plane experiencing the maximum shear stress range. The influence of accompanying normal stress on this plane is incorporated through the multiaxiality parameter ρ_w, as defined in Eq. 5 [7,21,26,30–32]:

$$\rho_w = \frac{\Delta\sigma_n}{\Delta\tau} \quad (5)$$

where $\Delta\sigma_n$ is the maximum normal stress range on the critical plane and $\Delta\tau$ is the corresponding maximum shear stress range. Here, ρ_w=1 corresponds to uniaxial loading and ρ_w=0 represents pure torsional loading. This method is typically visualised using a modified Wöhler diagram, where shear stress range $\Delta\tau$ is plotted against fatigue life, N_f as shown in Fig. 9 [26,30,33].

From this diagram, two critical parameters are identified: the negative inverse slope, k_τ and the reference shear stress range, $\Delta\tau_{R,MWCM}$. These parameters are both interpolated as linear functions calibrated using uniaxial and pure torsional reference fatigue curves as defined in Eqs 6 and 7, respectively [7,21,26,30–32].

$$k_\tau(\rho_w) = [k_\tau(\rho_w = 1) - k_\tau(\rho_w = 0)]\rho_w + k_\tau(\rho_w = 0) \quad (6)$$

$$\Delta\tau_{R,MWCM}(\rho_w) = \left(\frac{\Delta\sigma_R}{2} - \Delta\tau_R\right)\rho_w + \Delta\tau_R \quad (7)$$

To prevent excessive conservatism at high ρ_w, a limiting threshold applied as in Eq. 8 [26,32].

$$\rho_{w,lim} = \frac{\Delta\tau_R}{2\Delta\tau_R - \Delta\sigma_R} \quad (8)$$

This correction ensures more realistic fatigue life estimations across different multiaxial loading conditions.

For all three criteria, once the criterion-specific equivalent stress range is determined, the estimated fatigue life is calculated using a unified power-law equation as in Eq. 9.

$$N_{f,e} = N_R \cdot \left(\frac{\Delta\sigma_R}{\Delta\sigma_{criterion}}\right)^k \quad (9)$$

In this formulation, $\Delta\sigma_{criterion}$ represents the equivalent stress or shear stress range defined by each fatigue criterion - namely, the IIW equivalent stress range, the maximum principal stress range, or the MWCM shear-based equivalent range, evaluated using the selected stress analysis approach. The terms $\Delta\sigma_R$ and k denote the reference fatigue strength and negative inverse slope of the adopted S-N curve. This generalised formulation allows direct comparison of fatigue life estimates between criteria and forms the basis for comparative evaluation in the subsequent sections.

9. Validation Methodology

This section describes the procedure used to evaluate the predictive capability of the selected multiaxial fatigue criteria when applied to coldArc®-welded aluminium-to-steel tubular joints under CA loading.

The experimental dataset includes uniaxial, pure torsional, in-phase, and 90° out-of-phase multiaxial tests, all of which consistently showed that crack initiation occurred on the aluminium side.

All fatigue data used for validation including S-N curves, reference fatigue strengths, and negative inverse slopes were obtained either from standard reference fatigue strength values from the IIW and EC9 or from the experimentally derived parameters established for the tested hybrid joints. In this study, the term "standard parameters" refers to those FAT classes, slopes, and comparison values (CV) specified in IIW and EC9 recommendations, while "calibrated experimental parameters" refer to experimentally derived values from the tested welded joints. For the IIW-based evaluations, a constant CV of 1.0 was adopted, consistent with the IIW recommendations for aluminium welded joints under both proportional and non-proportional loading [5]. These values serve as the basis for all subsequent fatigue life estimations. These parameters include both the P_s of 97.7% reference fatigue strength and the common fitted slope k, obtained using log–log regression analysis.

Three multiaxial fatigue criteria were selected based on findings from the authors' prior quantitative reviews on fatigue modelling for welded aluminium and steel joints [3,4]. The NS approach was applied with IIW and EC9, reflecting standard practice in structural design. The MWCM was applied using the FNR and TCD PM stress fields, as these approaches provide the local stress information required by critical plane criteria. Additionally, the IIW recommendation is validated against the FNR approach within a local notch stress model. For the local notch stress analyses, the FNR concept was adopted following the latest IIW recommendations [5]. Given the thin-walled nature of the present aluminium weld, the reduced fictitious notch radius of 0.05 mm recommended by IIW for thin welded joints was used. This radius reflects fracture-mechanics-based developments for thin welds and was used in the present study together with the corresponding IIW-recommended reference fatigue strength for the governing critical region [5,15,22,34].

To assess the performance and accuracy of the fatigue criteria with stress analysis approaches in estimating fatigue life, fatigue life estimates were compared with experimental results using three key metrics: the percentage of non-conservative predictions (P_{NC}), the percentage of conservative predictions (P_C), and the root mean square error metric (T_{RMS}). The P_{NC} measure the proportion of predictions that underestimate fatigue life, while P_C quantifies overestimation. T_{RMS}, calculated from the root mean squared logarithmic error (RMSLE), provides an objective measure of estimation scatter across datasets as shown in Eq. 1:

$$RMSLE = \sqrt{\frac{\sum_{i=1}^{n}\left[\left(log\frac{N_{f(i)}}{N_{f,e(i)}}\right)^2\right]}{n}} \quad (10)$$

where $N_{f(i)}$ and $N_{f,e(i)}$ represent the experimental and estimated number of cycles to failure for each test i, and n is the total number of observations in each dataset. Whereas the T_{RMS} metric, defined in Eq. 2, provides further assessment of the deviation between estimated and experimental fatigue life results.

$$T_{RMS} = 10^{RMSLE} \quad (11)$$

Fatigue life estimates are classified as conservative (above the widest scatter band, P_s=97.7%) or non-conservative (below the scatter band, P_s=2.3%). These thresholds ensure a consistent and meaningful evaluation of multiaxial fatigue criterion reliability and safety.

10. Fatigue Life Estimation

This section presents the fatigue life estimations obtained using the selected multiaxial fatigue criteria in combination with three stress-analysis approaches: NS, FNR, and TCD-PM. For each approach–criterion, estimated fatigue lives were compared against experimental results under uniaxial, torsional, and multiaxial loading conditions. Performance is illustrated using fatigue life plots that incorporate both standard reference curve constants and experimentally calibrated parameters obtained from the same welded joint configuration in a related study. This enables a direct evaluation of each method's predictive accuracy and scatter, providing insight into how modelling choices influence estimation reliability across different loading scenarios.

10.1 Reanalysis using the NS approach

The NS approach remains one of the most practical and widely adopted method for stress analysis due to its simplicity, ease of implementation, and alignment with established design codes [2,5]. In this study, fatigue life estimations were performed using the IIW and EC9 criteria, both applied to nominal axial and shear stress components.

Fig. 10 presents the estimated fatigue lives obtained using both standard code-based parameters and experimentally derived fatigue strengths for IIW and EC9. These predictions are benchmarked against experimental data encompassing uniaxial, pure torsional, in-phase, and 90° out-of-phase multiaxial loading conditions. All data points are plotted together to assess the criteria's performance across different load paths. Specifically, Figs 10a and 10b show the fatigue life estimates for the IIW criterion using standard and experimental parameters, respectively, while Figs 10c and 10d present corresponding results for the EC9 criterion.

Although the uniaxial and pure torsional tests form the form the experimental datasets used for calibration, their inherent experimental scatter prevents a perfect alignment of all corresponding

estimated fatigue lives on the P_s of 50% middle line. Instead, these cases cluster around the diagonal line, with their mean lying close to the P_s of 50% curve, reflecting the natural variability of welded-joint fatigue data.

Both EC9 and IIW exhibited reasonable agreement with experimental fatigue life, with most of the points falling within the widest P_s of 2.3 and 97.7% uniaxial scatter bands. The use of experimentally calibrated parameters led to noticeable reductions in scatter and improved estimation accuracy. Among these two criteria, the EC9 criterion exhibits slightly less conservative predictions for pure torsion but provides the most accurate estimates for all other loading conditions. This is confirmed by its lowest average T_{RMS} values making it the most reliable NS approach-based fatigue criterion. On the other hand, the IIW criterion is slightly more conservative than the EC9 criterion, especially under out-of-phase loading using the standard IIW-recommended parameters with CV of 1.0. Nonetheless, the IIW criterion remains highly effective, as it performs exceptionally well under pure torsional loading conditions, reinforcing its applicability for multiaxial fatigue assessment.

Importantly, neither criterion exhibited marked sensitivity to loading proportionality, aligning with experimental findings in section 4 that highlighted the fatigue performance of coldArc®-welded hybrid joints is largely unaffected by non-proportional loading. Most predictions were either within or above the reference scatter band, indicating a conservative trend, especially when using standard fatigue parameters.

In summary, both the IIW and EC9 criteria, when used with the NS approach, offer practical and relatively safe fatigue life estimations for coldArc®-welded aluminium-to-steel joints under multiaxial loading. However, NS approach has its limitation in situations where the nominal reference area is no longer straightforward to be defined for complex welded joint geometries, motivating the use of localised stress analysis approaches which will be explored in subsequent sections [5,18,35–37].

10.2 Reanalysis using the FNR approach

The FNR approach adopted in this study follows the IIW recommendations for evaluating local notch stresses in thin-walled welded joints [5]. Local stress fields were extracted from the FE model described in Section 7 were assessed using three multiaxial fatigue criteria: IIW, the Maximum Principal (MP) stress criterion (used here as a substitute for EC9), and the MWCM. The EC9 criterion is referred to as the MP criterion in this context, as it lacks explicit guidance in the EC9 for application with ENS approach [2]. The fatigue life graphs showing the distribution of the fatigue life estimates based on both standard and experimental parameters are shown in Fig. 11. As with the NS approach analysis, the use of experimentally derived fatigue constants consistently improved estimation accuracy and reduced prediction scatter.

Among the criteria, the IIW approach produced the most accurate fatigue life estimates when used with experimental constants, yielding the lowest T_{RMS} values across all loading conditions, as shown in Fig. 11b. The MP criterion also performed reliably but exhibited slightly higher scatter. The MWCM showed good predictive capability when applied with standard parameters, particularly for in-phase and out-of-phase multiaxial loading, where it exhibited comparatively low scatter relative to the other criteria. When experimentally derived parameters were used, the performance of the MWCM remained generally consistent across load paths but did not show a systematic advantage over the other criteria for out-of-phase loading cases.

Overall, the FNR approach enhanced the reliability of fatigue life estimation by capturing localised stress states, which are essential for accurate assessment of hybrid welded joints.

10.3 Reanalysis using the TCD approach

The TCD approach applied here in its simplest form via the PM, is used as an alternative local stress-based approach in conjunction with the MWCM criterion to reanalyse the fatigue behaviour of the hybrid welded joints [25,26,31,32,38]. As detailed earlier in Sections 6 and 7, this approach treats weld toes and roots as sharp notches and evaluates the stress at a material-dependent critical distance.

Since the MWCM is already optimised and calibrated for use with the TCD PM, no additional fatigue criteria are considered here [25,26,31,32,38]. The corresponding fatigue life estimations are presented in Fig. 12. Results indicate that the TCD PM yields consistently conservative and safe predictions across all loading conditions. Despite assuming idealised notch sharpness, the level of conservatism remains within acceptable limits, and the accuracy of fatigue life estimation is satisfactory.

This performance is notable given that the original calibration of the M-D_v was based on aluminium cruciform joints with significantly different geometries and thicknesses [26,39]. The successful application of this method to hybrid joints without additional recalibration highlights its robustness and adaptability. Furthermore, since the TCD PM is already a validated design method for aluminium welded joints, its extension to hybrid aluminium-to-steel configurations supports its practical relevance for engineering applications.

In summary, the TCD PM with MWCM offers a provides a reliable alternative for multiaxial fatigue assessment of welded joints. Its main practical advantage is that it eliminates the need to define and model a fictitious notch radius for every weld toe and root - an otherwise labour-intensive step for complex geometries with multiple potential initiation sites, because the method evaluates the sharp-notch stress field through a material-dependent critical distance. While the approach still requires a refined mesh near stress singularities, this requirement is comparable to other local stress methods. The next section provides a comparative discussion of all stress analysis approaches, NS, FNR, and TCD PM, highlighting their relative performance and implications for reliable fatigue assessment.

11. Discussion

The experimental programme and subsequent multiaxial reanalyses collectively clarify the fatigue behaviour of coldArc®-welded aluminium-to-steel tubular joints and the effectiveness of different stress-analysis and fatigue-assessment strategies. Across all loading conditions, fatigue cracks initiated exclusively on the aluminium side, predominantly at the weld toe, confirming that fatigue performance is governed by the aluminium material and its local geometric discontinuities. Accordingly, both the fatigue assessment and stress analysis approaches can justifiably focus on the aluminium region, while the steel component primarily contributes to global load-bearing capacity.

Another key finding was the negligible influence of non-proportional fatigue loading. Fatigue life did not significantly deteriorate under 90° out-of-phase conditions compared to in-phase loading, regardless of λ. This contrasts with steel welded joints, where non-proportional loading typically increases damage accumulation. The results align with previous studies showing that the semi-ductile nature of aluminium mitigates the damaging effects of principal stress rotation. These results support the use of a CV of 1.0, as recommended by the IIW for aluminium welded joints [5]. Although the joint configuration is hybrid, the fatigue behaviour and failure assessment are governed by the aluminium side. Therefore, simplified multiaxial fatigue models that do not explicitly account for non-proportional loading, such as those recommended in EC9 and the IIW, remain effective for the present joint configuration.

Mean stress effects were found to be modest but not negligible. The re-evaluated S–N data using a common slope showed a reduction in fatigue strength at $R = 0.1$ relative to $R = -1$, with the effect being more pronounced under uniaxial loading than torsional loading. This trend reflects the dominant role of tensile stresses in promoting crack opening and accelerating fatigue damage under normal stress conditions, whereas shear-dominated loading is less sensitive to mean stress variations. Although residual stresses were not experimentally measured in this study, previous investigations on as-welded aluminium and steel joints have consistently reported high tensile residual stresses near the weld toe and root. Such residual stresses elevate the local effective stress ratio, partially offsetting the influence of externally applied mean stresses. Therefore, the limited mean stress sensitivity observed in the present hybrid joints can be reasonably attributed to this residual stress state, in agreement with established findings for as-welded configurations in Eurocodes and the IIW [1,2,5].

The effect of biaxiality ratio was also evident. Reducing λ from $\sqrt{3}$ to 1, which increases the proportion of applied shear stress relative to normal stress, led to a consistent decrease in fatigue strength. This reduction arises because the endurable shear stress of welded joints is inherently lower than the corresponding normal stress capacity. Consequently, as the shear contribution becomes more dominant,

crack initiation is promoted along shear-dominated planes, accelerating fatigue damage and shortening fatigue life.

The performance of the NS, FNR, and TCD PM stress analysis approaches was compared, based on their effectiveness in estimating the fatigue life of coldArc®-welded aluminium-to-steel hybrid joints. Drawing on results from the reanalyses, it highlights key trends across multiaxial fatigue criteria and considers practical implications for fatigue assessment and structural design. Comparative metrics for the top three criteria under each approach are provided in Tab. 4.

The NS approach, although simple and widely adopted, demonstrated strong reliability when paired with established criteria such as EC9 or MP and IIW. These combinations yielded conservative and consistent predictions, especially under uniaxial and proportional multiaxial loading. The continued viability of nominal stress methods is reinforced, particularly for structures with well-defined load paths and standard weld geometries where detailed local stress modelling is not feasible.

In contrast, FNR-based approaches allowed for a more detailed representation of stress concentrations at weld toes and roots, offering improved fatigue life estimation across all criteria. In particular, the IIW criterion consistently produced accurate and low-scatter predictions, confirming its robustness when local stress conditions are accounted for. These findings underscore the benefit of using local stress

The TCD PM provides an alternative local stress evaluation method by assuming zero-radius notches and using a fixed material-specific critical distance. When combined with the MWCM criterion, it achieved safe and consistent predictions across all loading paths without requiring explicit modelling of weld toe or root radii. Although originally calibrated for homogeneous aluminium and steel welded joints, the method transferred effectively to the present hybrid configuration. Importantly, because TCD does not rely on weld profile measurements, it can be advantageous in applications where detailed geometry characterisation is impractical or unavailable. This limitation similarly motivates the use of standardised fictitious notch radii in IIW-recommended FNR approaches, while still offering conservative fatigue assessments.

Across all methods, fatigue life predictions made using standard reference strengths remained safely conservative. Given that these standard reference fatigue curve parameters are typically based on lower-grade aluminium alloys, the slightly conservative results for AA6082-T6 were expected. This reinforces the suitability of existing design curves and fatigue parameters for structural applications involving higher-strength aluminium components, without compromising safety margins.

Overall, these findings clarify the relative strengths and practical trade-offs of each stress analysis method and support the selection of fatigue criteria and modelling strategies appropriate to different levels of design complexity.

12. Conclusions

This study experimentally characterised and assessed the multiaxial fatigue behaviour of coldArc®-welded thin aluminium-to-steel tubular joints using three stress analysis approaches - NS, FNR, and TCD PM - in combination with established multiaxial fatigue criteria. The main conclusions are:

- Fatigue cracks consistently initiated in the aluminium component, particularly at the aluminium weld toe and WR2 with no failures detected on the steel side. Aluminium is therefore the fatigue-critical region of these hybrid joints.
- Re-evaluation of the S–N data with a common slope showed that fatigue strength at R = 0.1 is approximately 15–20% lower than at R = -1 at 2 million cycles. This indicates a modest mean-stress effect, with the influence being more pronounced under uniaxial than under torsional loading.
- No significant degradation in fatigue strength was observed under 90° out-of-phase loading compared to in-phase conditions. This limited sensitivity to non-proportionality supports the use of fatigue criteria recommended by standards such as EC9 and the IIW under multiaxial loading.
- The FNR approach improved prediction accuracy by capturing local stress concentrations using the fictitious notch radius of 0.05mm for thin welded joints recommended by the IIW.
- When used with the MWCM, the TCD PM approach provided consistently conservative fatigue life estimates across all loading paths. While based on the sharp-notch assumption, the use of critical distance removes the need to introduce fictitious weld toe or root radii and produced prediction trends comparable to the FNR model, making TCD PM a practical alternative for multiaxial fatigue assessment of welded joints.
- Among all criteria, the IIW criterion delivered the most accurate and consistent predictions, and the EC9 criterion performed well under the NS approach. The MWCM, while generally slightly less accurate than IIW and EC9, remained applicable when combined with localised stress analysis approaches and offered a viable basis for interpreting multiaxial loading effects, albeit with higher calculation effort.

Together, these findings clarify how established multiaxial fatigue criteria and stress analysis approaches perform when applied to hybrid aluminium-to-steel welded joints. The results show that conventional methodologies can be appropriately adapted to this joint configuration, providing practical guidance for reliable fatigue assessment in engineering applications.

References

[1] Anon. Eurocode 3: Design of steel structures — Part 1-9: Fatigue . 2005.

[2] Anon. Eurocode 9: Design of aluminium structures — Part 1-3: Structures susceptible to fatigue . 2007.

[3] Ng CT, Susmel L. Quantitative Review of Critical Plane Criteria and Stress Analysis Approaches for Multiaxial Fatigue of Welded Joints. Fatigue Fract Eng Mater Struct 2025;48:1393–428. https://doi.org/https://doi.org/10.1111/ffe.14571.

[4] Ng CT, Sonsino CM, Susmel L. Multiaxial fatigue assessment of welded joints: A review of Eurocode 3 and International Institute of Welding criteria with different stress analysis approaches. Fatigue Fract Eng Mater Struct 2024.

[5] Hobbacher AF, Baumgartner J. Recommendations for fatigue design of welded joints and components. Springer; 2024.

[6] Susmel L. The Modified Wöhler Curve Method calibrated by using standard fatigue curves and applied in conjunction with the Theory of Critical Distances to estimate fatigue lifetime of aluminium weldments. Int J Fatigue 2009;31:197–212. https://doi.org/10.1016/j.ijfatigue.2008.04.004.

[7] Susmel L, Askes H. Modified Wöhler Curve Method and multiaxial fatigue assessment of thin welded joints. Int J Fatigue 2012;43:30–42. https://doi.org/10.1016/j.ijfatigue.2012.01.026.

[8] Bäckström M, Marquis G. A review of multiaxial fatigue of weldments: experimental results, design code and critical plane approaches. Fatigue Fract Eng Mater Struct 2001;24:279–91.

[9] Shen W, Yan R, He F, Wang S. Multiaxial fatigue analysis of complex welded joints in notch stress approach. Eng Fract Mech 2018;204:344–60. https://doi.org/10.1016/j.engfracmech.2018.10.035.

[10] Meneghetti G, Campagnolo A, Babini V, Riboli M, Spagnoli A. Multiaxial fatigue assessment of welded steel details according to the peak stress method: Industrial case studies. Int J Fatigue 2019;125:362–80. https://doi.org/10.1016/j.ijfatigue.2019.04.014.

[11] Al Zamzami I, Davison B, Susmel L. Nominal and local stress quantities to design aluminium-to-steel thin welded joints against fatigue. Int J Fatigue 2019;123:279–95.

[12] Al Zamzami I, Di Cocco V, Davison JB, Iacoviello F, Susmel L. Static strength and design of aluminium-to-steel thin welded joints. Weld World 2018;62:1255–72. https://doi.org/10.1007/s40194-018-0634-2.

[13] Meilinger Á, Cserépi MF, Lukács J. Behaviour of aluminium/steel hybrid RSW joints under high cycle fatigue loading. Weld World 2024;68:427–40.

[14] Ng CT, Susmel L. Failure analysis of hybrid Aluminium-to-Steel welded joints under Uniaxial/Multiaxial fatigue loading. Eng Fail Anal 2024;163:108529. https://doi.org/https://doi.org/10.1016/j.engfailanal.2024.108529.

[15] Sonsino CM, Bruder T, Baumgartner J. SN lines for welded thin joints—suggested slopes and FAT values for applying the notch stress concept with various reference radii. Weld World 2010;54:R375–92.

[16] Sonsino CM, Fricke W, De Bruyne F, Hoppe A, Ahmadi A, Zhang G. Notch stress concepts for the fatigue assessment of welded joints–Background and applications. Int J Fatigue 2012;34:2–16.

[17] Atzori B. Trattamenti termici e resistenza a fatica delle strutture saldate. Riv Ital Saldat, edited by A.T.A., Genova, Italy, 1983;1:3–16.

[18] Susmel L, Tovo R. On the use of nominal stresses to predict the fatigue strength of welded joints under biaxial cyclic loading. Fatigue Fract Eng Mater Struct 2004;27:1005–24.

[19] Kueppers M, Sonsino CM. Critical plane approach for the assessment of the fatigue behaviour of welded aluminium under multiaxial loading. Fatigue Fract Eng Mater Struct 2003;26:507–13.

[20] Kueppers M, Sonsino CM. Assessment of the fatigue behaviour of welded aluminium joints under multiaxial spectrum loading by a critical plane approach. Int J Fatigue 2006;28:540–6.

[21] Al Zamzami I, Susmel L. On the use of hot-spot stresses, effective notch stresses and the Point Method to estimate lifetime of inclined welds subjected to uniaxial fatigue loading. Int J Fatigue 2018;117:432–49. https://doi.org/10.1016/j.ijfatigue.2018.08.032.

[22] Sonsino CM, Fricke W, De Bruyne F, Hoppe A, Ahmadi A, Zhang G. Notch stress concepts for the fatigue assessment of welded joints–Background and applications. Int J Fatigue 2012;34:2–16.

[23] Lazzarin P, Tovo R. A notch intensity factor approach to the stress analysis of welds. Fatigue Fract Eng Mater Struct 1998;21:1089–103.

[24] Lazzarin P, Livieri P. Notch stress intensity factors and fatigue strength of aluminium and steel welded joints. vol. 23. 2001.

[25] Susmel L. Eurocode 3's standard curves and theory of critical distances to estimate fatigue lifetime of steel weldments. Key Eng Mater 2007;348:21–4.

[26] Susmel L. Multiaxial Notch Fatigue. vol. 81. Elsevier; 2009. https://doi.org/10.1108/aeat.2009.12781dae.001.

[27] Pedersen MM. Multiaxial fatigue assessment of welded joints using the notch stress approach. Int J Fatigue 2016;83:269–79. https://doi.org/10.1016/J.IJFATIGUE.2015.10.021.

[28] Mei J, Dong P. An equivalent stress parameter for multi-axial fatigue evaluation of welded components including non-proportional loading effects. Int J Fatigue 2017;101:297–311.

[29] Mei J, Dong P, Xing S, Vasu A, Ganamet A, Chung J, et al. An overview and comparative assessment of approaches to multi-axial fatigue of welded components in codes and standards. Int J Fatigue 2021;146:106144.

[30] Susmel L, Lazzarin P. A bi-parametric Wöhler curve for high cycle multiaxial fatigue assessment. Fatigue Fract Eng Mater Struct 2002;25:63–78.

[31] Susmel L. Three different ways of using the Modified Wöhler Curve Method to perform the multiaxial fatigue assessment of steel and aluminium welded joints. Eng Fail Anal 2009;16:1074–89. https://doi.org/10.1016/j.engfailanal.2008.05.016.

[32] Susmel L. Four stress analysis strategies to use the Modified Wöhler Curve Method to perform the fatigue assessment of weldments subjected to constant and variable amplitude multiaxial fatigue loading. Int J Fatigue 2014;67:38–54. https://doi.org/10.1016/j.ijfatigue.2013.12.001.

[33] Susmel L, Tovo R, Benasciutti D. A novel engineering method based on the critical plane concept to estimate the lifetime of weldments subjected to variable amplitude multiaxial fatigue loading. Fatigue Fract Eng Mater Struct 2009;32:441–59. https://doi.org/10.1111/j.1460-2695.2009.01349.x.

[34] Sonsino CM. Multiaxial fatigue assessment of welded joints–recommendations for design codes. Int J Fatigue 2009;31:173–87.

[35] Niemi E. Stress determination for fatigue analysis of welded components. Woodhead Publishing; 1995.

[36] Sonsino CM. Multiaxial fatigue of welded joints under in-phase and out-of-phase local strains and stresses. Int J Fatigue 1995;17:55–70.

[37] Radaj D, Sonsino CM, Fricke W. Fatigue assessment of welded joints by local approaches. Woodhead publishing; 2006.

[38] Taylor D, Barrett N, Lucano G. Some new methods for predicting fatigue in welded joints. vol. 24. 2002.

[39] Livieri P, Lazzarin P. Fatigue strength of steel and aluminium welded joints based on generalised stress intensity factors and local strain energy values. Int J Fract 2005;133:247–76.

List of Captions

Table 1. Experimental constant amplitude (CA) fatigue data for aluminium-to-steel welded joints, including nominal stress ranges, stress ratios, phase angles, and cycles to failure.

Table 2. Reference fatigue strengths and corresponding negative inverse slopes for uniaxial and torsional loading, derived using different stress analysis approaches for hybrid aluminium-to-steel welded joints.

Table 3. Stress concentration factors (SCFs) derived from finite element analysis for the governing fatigue-critical location associated with the FNR and TCD-PM stress analysis approaches under uniaxial and torsional loading.

Table 4. Summary of P_{NC}, P_C, and T_{RMS} values showing fatigue life estimation performance, using various stress analysis approaches with different multiaxial fatigue criteria.

Figure 1. Geometry of the coldArc®-welded aluminium-to-steel joint specimens: (a) AA6082-T6 aluminium section, (b) S235 steel section, and (c) assembled hybrid joint configuration.

Figure 2. Applied fatigue loading paths for uniaxial, pure torsional, in-phase, and 90° out-of-phase configurations.

Figure 3. Fatigue-critical weld features and corresponding geometric representation: overview of the welded joint and locations of detailed observations (a), aluminium weld toe (b), steel weld toe (c), weld root region showing WR1 and WR2 (d), and representation in the Fictitious Notch Radius (FNR) finite element model (e).

Figure 4. Example illustrating the determination of experimental crack initiation and experimental crack propagation angles under in-phase loading.

Figure 5. S–N curves for aluminium-to-steel welded joints under uniaxial (a, c) and pure torsional (b, d) loading. Figures (a) and (b) show regression fits for R=-1 fatigue data; (c) and (d) overlay R = 0.1 results onto the corresponding R = -1 scatter bands using parallel slopes to illustrate mean-stress sensitivity.

Figure 6. S–N curves under in-phase and out-of-phase fatigue loading at $\lambda=1$ and $\lambda=\sqrt{3}$, illustrating the influence of loading proportionality on fatigue strength.

Figure 7. S–N curves for aluminium-to-steel welded joints under (a) uniaxial and (b) torsional loading using the NS approach, and (c-d) the FNR approach. All plots include R = –1 and R = 0.1 fatigue data within the fitted scatter bands.

Figure 8. Finite element model of the weld region and representative maximum principal stress contours for (a) FNR and (b) TCD-PM approach, showing critical locations and focus paths from weld toe/root locations used in multiaxial fatigue assessment.

Figure 9. Modified Wöhler diagram used in the MWCM, showing the relationship between shear stress range ($\Delta\tau$), fatigue life (N_f), and the multiaxiality parameter (ρ_w).

Figure 10. Nominal Stress (NS) approach: fatigue life estimations for as-welded hybrid aluminium-to-steel joints with (a-b) IIW and (c-d) EC9 criteria, comparing standard and experimental reference strengths at P_s=50%.

Figure 11. Fictitious Notch Radius (FNR) approach: fatigue life estimations for as-welded hybrid aluminium-to-steel joints with (a-b) IIW, (c-d), and (e-f) MWCM criteria, comparing standard and experimental reference strengths at P_s=50%.

Figure 12. Fatigue life estimations for as-welded hybrid aluminium-to-steel joints using TCD PM approach with the MWCM, based on standard reference strength at P_s=50%.

Tables

Table 1. Experimental constant amplitude (CA) fatigue data for aluminium-to-steel welded joints, including nominal stress ranges, stress ratios, phase angles, and cycles to failure.

Code	$\Delta\sigma_{nom}$ [MPa]	$\Delta\tau_{nom}$ [MPa]	R_σ [1] [-]	R_τ [1] [-]	δ [2] [°]	N_f [Cycles]
U_T_1	112.4	0	-1	-	0	142470
U_T_2	116.2	0	-1	-	0	102215
U_T_3	91.8	0	-1	-	0	1684898
U_T_4	85.4	0	-1	-	0	1305955
U_T_5	143.5	0	-1	-	0	181007
U_T_6	138.2	0	-1	-	0	48990
U_T_7	218.3	0	-1	-	0	10892
U_T_8	229.9	0	-1	-	0	17562
U_T_9	101.2	0	0.1	-	0	95979
U_T_10	91.2	0	0.1	-	0	334167
U_T_11	144.5	0	0.1	-	0	20532
U_T_12	146.2	0	0.1	-	0	36170
P_To_1	0.0	173.7	-	-1	0	4912
P_To_2	0.0	181.5	-	-1	0	2851
P_To_3	0.0	106.8	-	-1	0	164727
P_To_4	0.0	104.9	-	-1	0	76790
P_To_5	0.0	75.8	-	-1	0	686004
P_To_6	0.0	76.6	-	-1	0	681711
P_To_7	0.0	132.6	-	-1	0	73458
P_To_8	0.0	127.9	-	-1	0	95737
P_To_9	0.0	81.2	-	0.1	0	284460
P_To_10	0.0	70.7	-	0.1	0	321082
P_To_11	0.0	103.8	-	0.1	0	109045
P_To_12	0.0	111.0	-	0.1	0	11122
C_I_U_To_1	68.9	68.9	-1	-1	0	375424
C_I_U_To_2	98.4	98.4	-1	-1	0	26492
C_I_U_To_3	100.4	100.4	-1	-1	0	132324
C_I_U_To_4	64.6	64.6	-1	-1	0	976928
C_I_U_To_5	63.2	63.2	-1	-1	0	997868
C_I_U_To_6	104.6	104.6	-1	-1	0	79265
C_I_U_To_6_1	45.4	45.4	-1	-1	0	2000000*
C_I_U_To_7	92.4	92.4	0.1	-1	0	43453

C_I_U_To_8	68.2	68.2	0.1	-1	0	425460
C_I_U_To_9	88.5	88.5	0.1	-1	0	41265
C_I_U_To_10	66.8	66.8	0.1	-1	0	250461
C_I_U_To_11	69.8	69.8	0.1	0.1	0	217322
C_I_U_To_12	77.6	77.6	0.1	0.1	0	146225
C_I_U_To_13	66.8	66.8	0.1	0.1	0	309597
C_I_U_To_14	83.0	83.0	0.1	0.1	0	96381
C_I_U_To_15	66.0	66.0	-1	0.1	0	366617
C_I_U_To_16	80.6	80.6	-1	0.1	0	138061
C_I_U_To_17	63.6	63.6	-1	0.1	0	379907
C_I_U_To_18	91.5	91.5	-1	0.1	0	141600
C_I_U_To_19	74.1	42.8	-1	-1	0	1263962
C_I_U_To_20	96.1	55.5	-1	-1	0	507067
C_I_U_To_21	136.1	78.6	-1	-1	0	162690
C_I_U_To_22	140.8	81.3	-1	-1	0	181957
C_I_U_To_23	173.3	100.1	-1	-1	0	27196
C_I_U_To_24	167.9	96.9	-1	-1	0	31616
C_I_U_To_25	86.0	49.7	-1	-1	0	484321
C_I_U_To_26	103.1	59.5	0.1	-1	0	151449
C_I_U_To_27	83.9	48.4	0.1	-1	0	1401080
C_I_U_To_28	102.2	59.0	0.1	-1	0	162502
C_I_U_To_29	90.7	52.4	0.1	-1	0	156933
C_I_U_To_30	83.1	48.0	0.1	0.1	0	108138
C_I_U_To_31	81.0	46.7	0.1	0.1	0	115647
C_I_U_To_32	89.3	51.6	0.1	0.1	0	101125
C_I_U_To_33	104.5	60.3	0.1	0.1	0	739803
C_I_U_To_34	128.3	74.1	-1	0.1	0	234227
C_I_U_To_35	99.7	57.6	-1	0.1	0	347373
C_I_U_To_36	126.6	73.1	-1	0.1	0	114846
C_O_U_To_1	97.3	97.3	-1	-1	90	245331
C_O_U_To_2	114.1	114.1	-1	-1	90	27707
C_O_U_To_3	111.1	111.1	-1	-1	90	52981
C_O_U_To_4	90.6	90.6	-1	-1	90	68432
C_O_U_To_5	90.4	90.4	-1	-1	90	164273
C_O_U_To_6	100.5	100.5	-1	-1	90	96411
C_O_U_To_7	101.2	101.2	0.1	-1	90	12867
C_O_U_To_8	82.0	82.0	0.1	-1	90	104377
C_O_U_To_9	100.0	100.0	0.1	-1	90	18207
C_O_U_To_10	78.2	78.2	0.1	-1	90	196031

C_O_U_To_11	86.2	86.2	0.1	0.1	90	163647
C_O_U_To_12	93.0	93.0	0.1	0.1	90	81558
C_O_U_To_13	88.2	88.2	0.1	0.1	90	53776
C_O_U_To_14	77.3	77.3	0.1	0.1	90	313637
C_O_U_To_15	91.4	91.4	-1	0.1	90	154696
C_O_U_To_16	92.3	92.3	-1	0.1	90	148405
C_O_U_To_17	77.2	77.2	-1	0.1	90	672474
C_O_U_To_18	84.1	84.1	-1	0.1	90	234437
C_O_U_To_19	108.3	62.5	-1	-1	90	430385
C_O_U_To_20	100.2	57.9	-1	-1	90	375500
C_O_U_To_21	165.1	95.3	-1	-1	90	114271
C_O_U_To_22	169.7	98.0	-1	-1	90	22815
C_O_U_To_23	173.0	99.9	-1	-1	90	20911
C_O_U_To_24	156.0	90.1	-1	-1	90	54050
C_O_U_To_25	100.5	58.0	-1	-1	90	93017
C_O_U_To_26	85.7	49.5	0.1	-1	90	368770
C_O_U_To_27	82.7	47.7	0.1	-1	90	183014
C_O_U_To_28	100.8	58.2	0.1	-1	90	73891
C_O_U_To_29	114.0	65.8	0.1	-1	90	57091
C_O_U_To_30	109.6	63.3	0.1	0.1	90	125012
C_O_U_To_31	98.5	56.9	0.1	0.1	90	539467
C_O_U_To_32	102.5	59.2	0.1	0.1	90	299370
C_O_U_To_33	138.7	80.1	0.1	0.1	90	185333
C_O_U_To_34	137.7	79.5	-1	0.1	90	52199
C_O_U_To_35	109.9	63.4	-1	0.1	90	390447
C_O_U_To_36	111.7	64.5	-1	0.1	90	246360

(1) R_σ and R_τ denote the stress ratio for normal and shear stress, respectively.

(2) δ represents out-of-phase angle for fatigue loading.

* Run-Out

Table 2. Reference fatigue strengths and corresponding negative inverse slopes for uniaxial and torsional loading, derived using different stress analysis approaches for hybrid aluminium-to-steel welded joints.

Stress Analysis Approach	$\Delta\sigma_{R,Ps=97.7\%}$ [(1)] (MPa)		Uniaxial curve slope, k		$\Delta\tau_{R,Ps=97.7\%}$ [(1)] (MPa)		Torsional curve slope, k0	
	Std[(2)]	Exp[(3)]	Std[(2)]	Exp[(3)]	Std[(2)]	Exp[(3)]	Std[(2)]	Exp[(3)]
NS	22	34.1	3	4.3	36	33.9	5	5.2
FNR	160	180.4	5	4.3	90	55.6	7	5.2
TCD	55	-	4.5	-	28	-	5	-

(1) Reference normal and shear stresses extrapolated at 2 million cycles to failure, with P_s=97.7%.
(2) Std refers to standard recommended values by IIW, EC9 and Sonsino's recommendations.
(3) Exp denotes experimental data.

Table 3. Stress concentration factors (SCFs) derived from finite element analysis for the governing fatigue-critical location associated with the FNR and TCD-PM stress analysis approaches under uniaxial and torsional loading.

Stress Analysis Approach	Governing Critical Notch Location	Stress Concentration Factors (SCFs)	
		K_{ta}[(1)]	K_{tt}[(2)]
FNR	Aluminium weld toe	5.30	1.64
TCD	Aluminium weld toe (0.075 mm from notch bisector)	2.30	1.04

(1) K_{ta} denote normal stress concentration factor under uniaxial loading.
(2) K_{tt} denote shear stress concentration factor under torsional loading.

Table 4. Summary of P_{NC}, P_C, and T_{RMS} values showing fatigue life estimation performance, using various stress analysis approaches with different multiaxial fatigue criteria.

Stress Analysis Approach	Condition	Multiaxial Fatigue Criterion	Standard[1]		Experimental[2]		$T_{RMS,Std}$[5]	$T_{RMS,Exp}$[6]
			P_{NC} (%)[3]	P_C (%)[4]	P_{NC} (%)[3]	P_C (%)[4]		
NS	Uniaxial	EC9	3.2	25.0	-	-	9.3	-
		IIW	0	50.0	-	-	31.8	-
	Torsional	EC9	25.0	0	8.3	0	10.3	20.6
		IIW	0	0	0	0	7.7	6.0
	In-Phase	EC9	0	41.7	0	0	30.6	12.9
		IIW	0	33.3	0	0	55.9	23.0
	Out-Of-Phase	EC9	5.6	16.7	0	0	6.5	7.2
		IIW	0	33.3	0	0	54.8	11.4
FNR	Uniaxial	IIW	0	66.7	-	-	365.7	-
		MP	0	66.7	-	-	364.8	-
		MWCM	0	50.0	-	-	239.7	-
	Torsional	IIW	16.7	0	-	-	28.8	-
		MP	16.7	0	-	-	28.9	-
		MWCM	16.7	0	-	-	29.0	-
	In-Phase	IIW	0	27.8	0	0	129.7	7.2
		MP	0	22.2	2.8	0	85.8	13.7
		MWCM	0	11.1	2.8	0	50.1	29.8
	Out-Of-Phase	IIW	0	33.3	0	0	185.5	7.7
		MP	0	19.4	0	0	70.7	18.7
		MWCM	0	13.9	5.6	0	47.2	41.3
TCD PM	Uniaxial	MWCM	0	33.3	-	-	48.8	-
	Torsional	MWCM	0	25.0	-	-	40.7	-
	In-Phase	MWCM	0	38.9	-	-	54.0	-
	Out-Of-Phase	MWCM	0	13.9	-	-	17.0	-

[1] Reanalysis using constants derived from standard reference curves.
[2] Reanalysis using constants derived from experimental reference curves.
[3] P_{NC} represents the percentage of non-conservative estimates.
[4] P_C represents the percentage of conservative estimates.
[5] $T_{RMS,Std}$ quantifies the error in fatigue life estimations when using constants from standard curves.
[6] $T_{RMS,Exp}$ quantifies the error in fatigue life estimations when using constants from experimental curves.

Figures

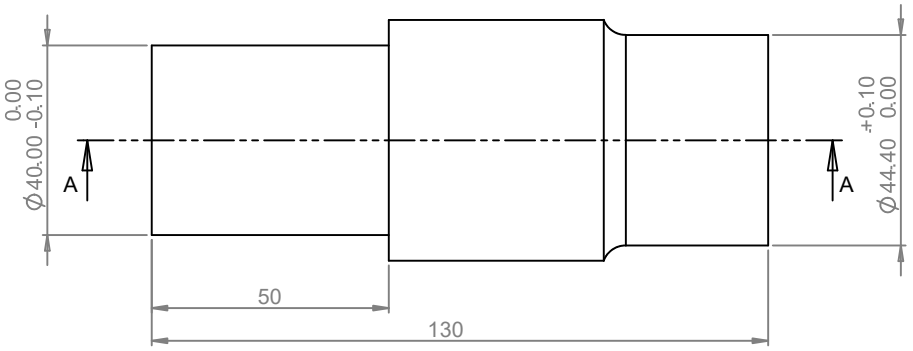

Front View

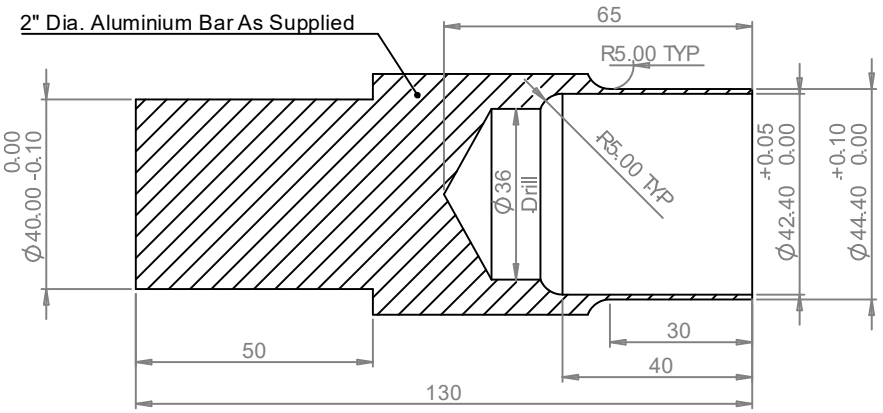

SECTION A-A

(a)

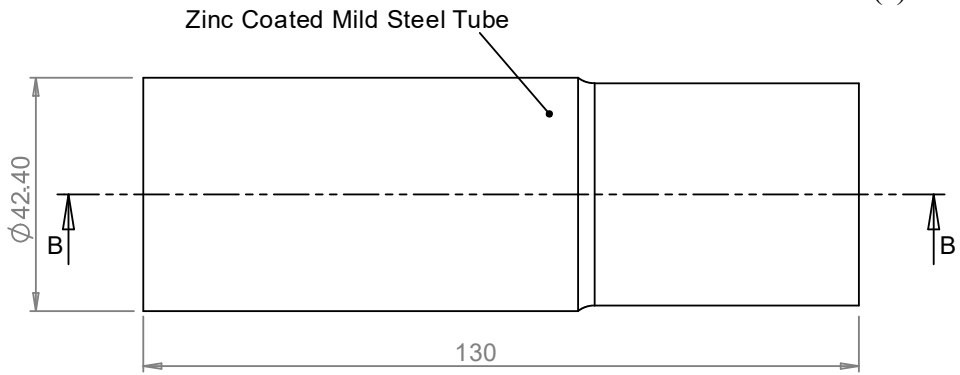

Front View

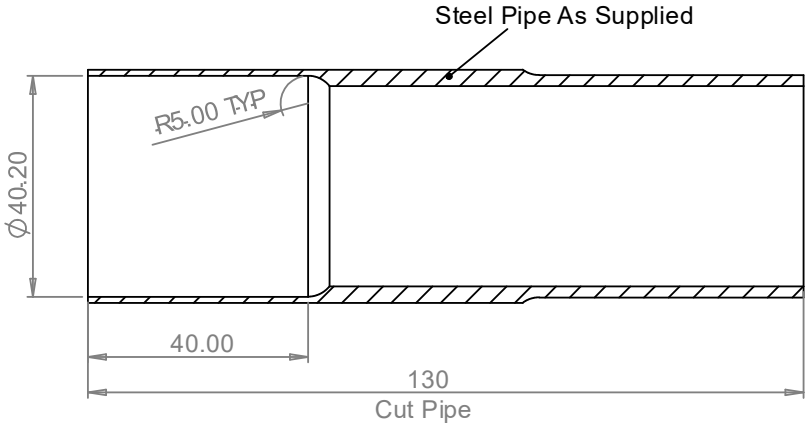

SECTION B-B

(b)

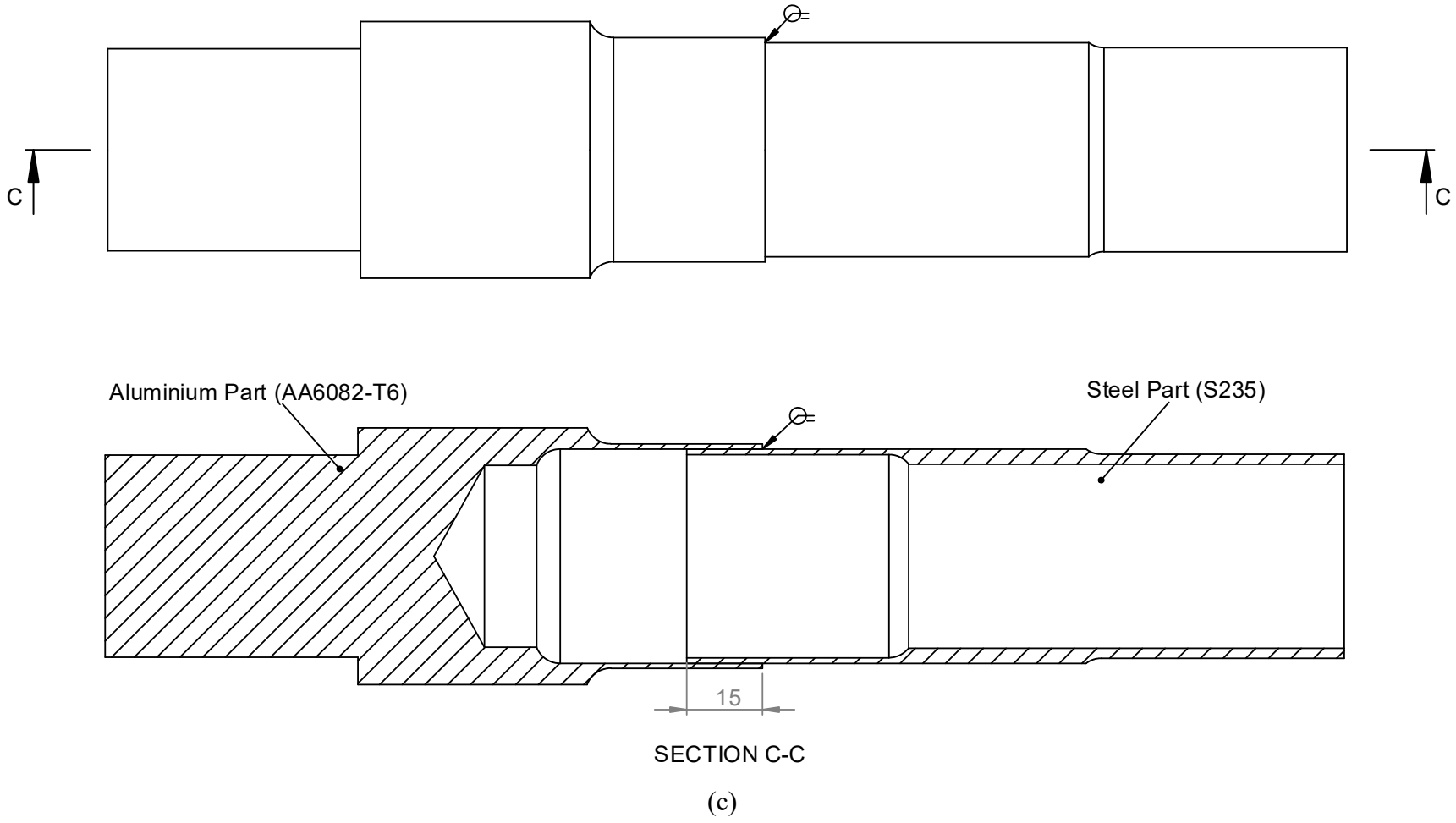

Figure 1. Geometry of the coldArc®-welded aluminium-to-steel joint specimens: (a) AA6082-T6 aluminium section, (b) S235 steel section, and (c) assembled hybrid joint configuration.

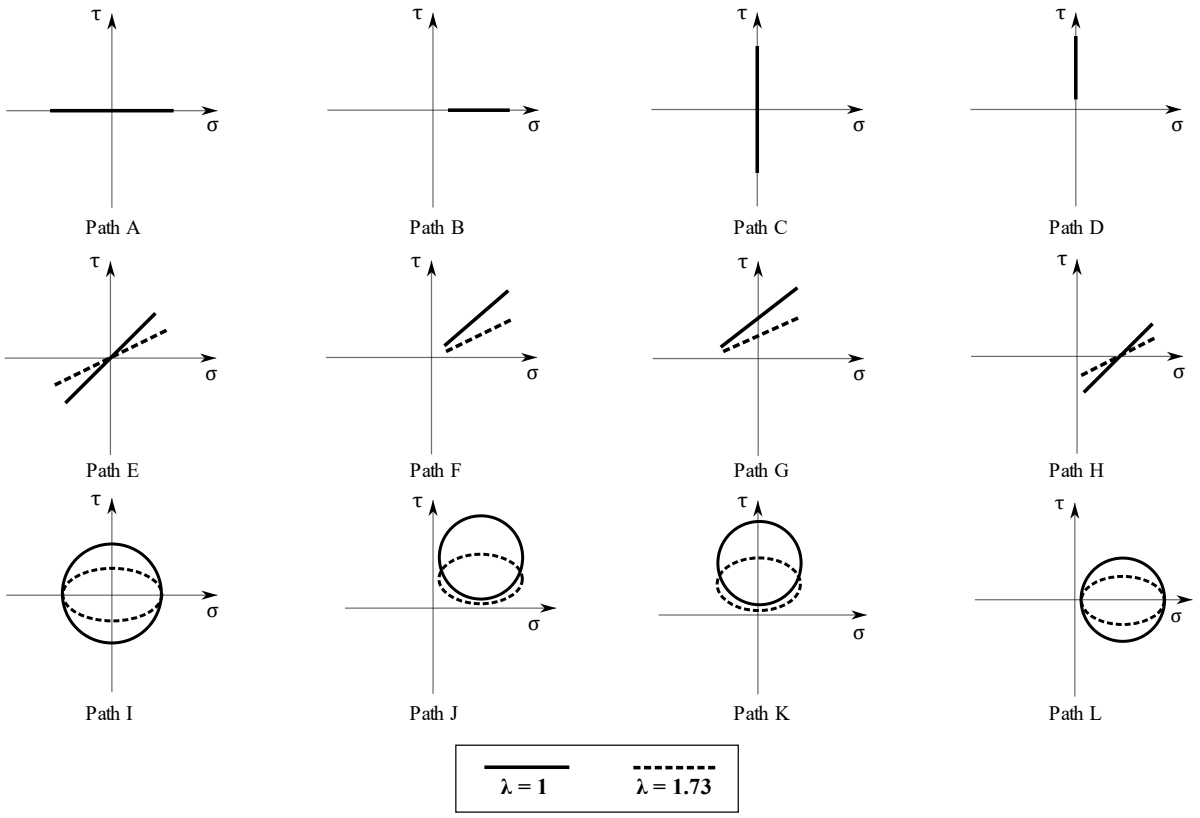

Figure 2. Applied fatigue loading paths for uniaxial, pure torsional, in-phase, and 90° out-of-phase configurations.

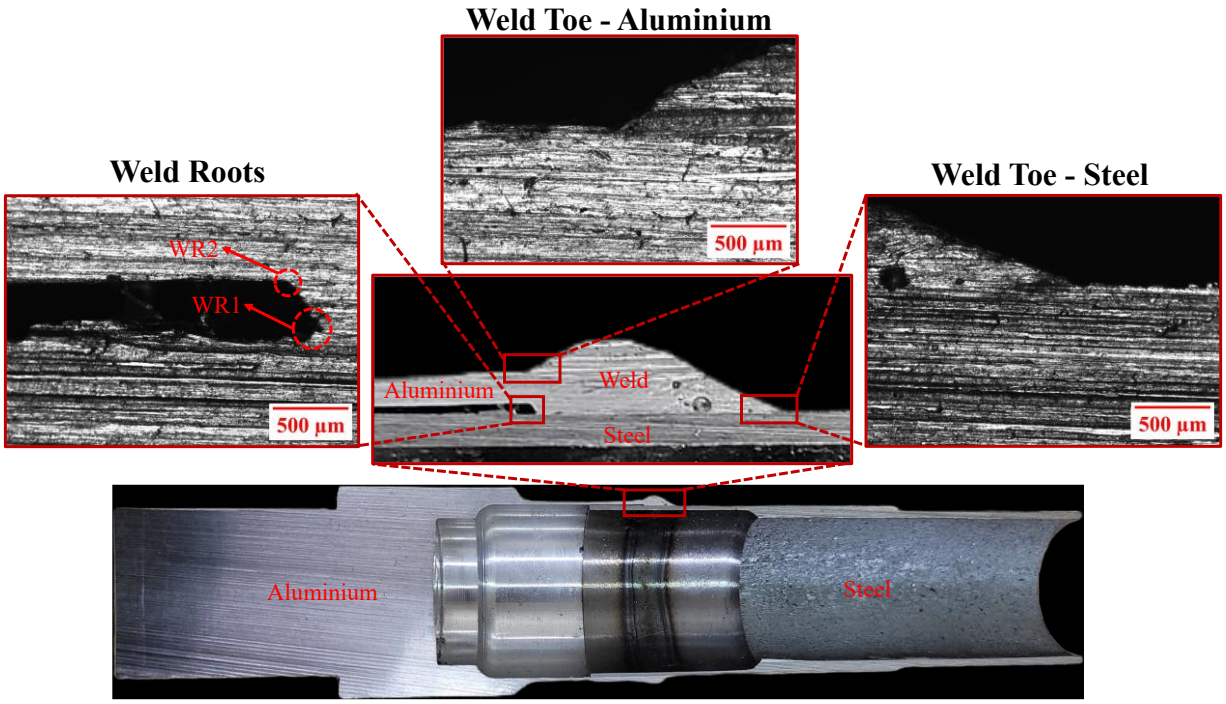
Weld Toe - Aluminium
Weld Roots
Weld Toe - Steel
WR2
WR1
500 µm
500 µm
500 µm
Aluminium
Weld
Steel
Aluminium
Steel

(a)

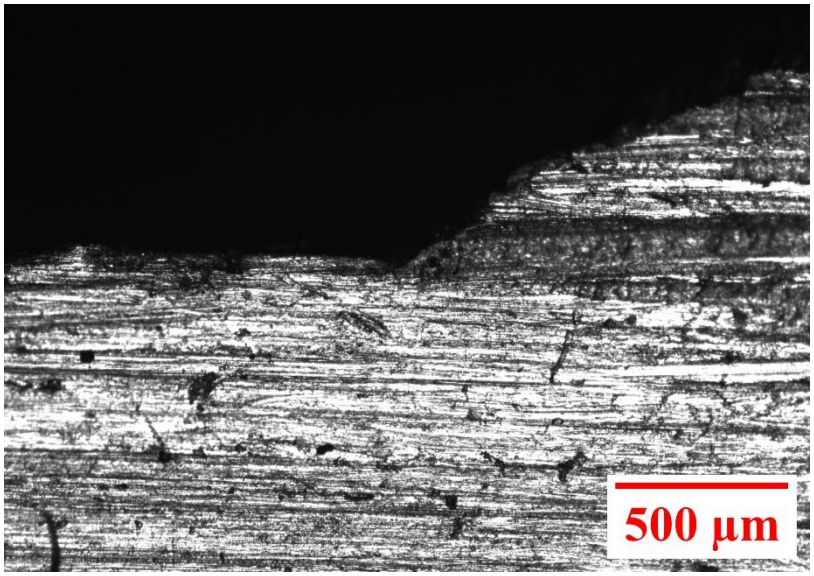
500 µm

(b)

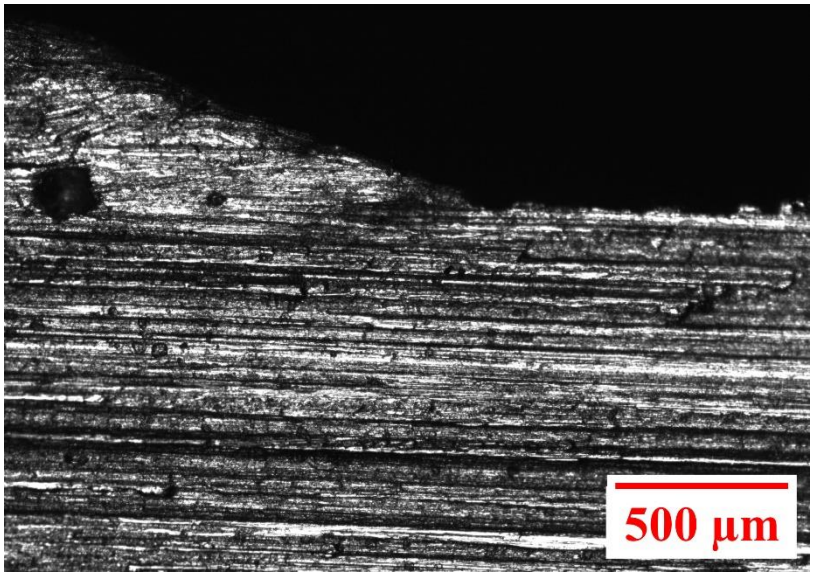

(c)

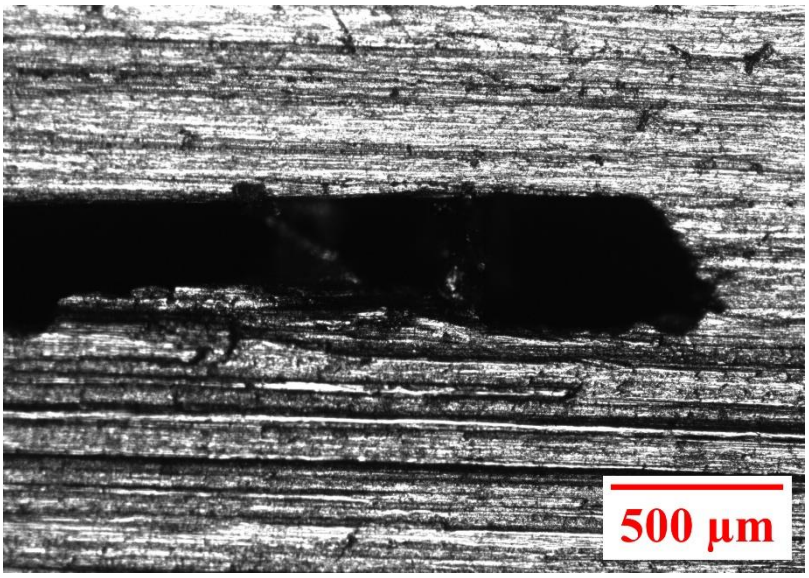

(d)

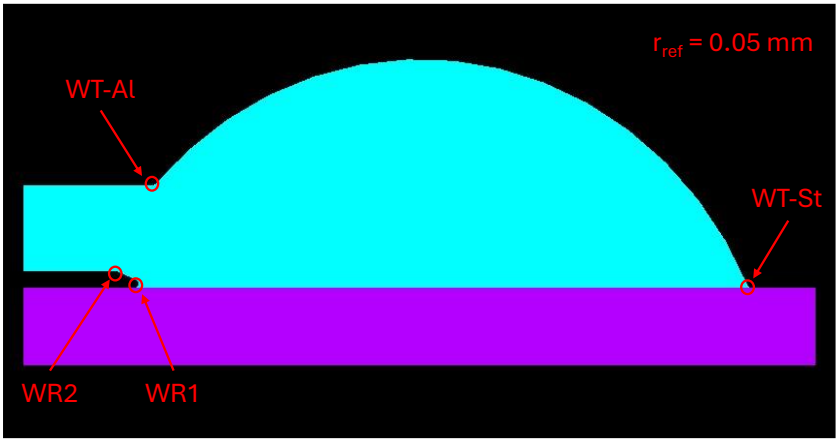

(e)

Figure 3. Fatigue-critical weld features and corresponding geometric representation: overview of the welded joint and locations of detailed observations (a), aluminium weld toe (b), steel weld toe (c), weld root region showing WR1 and WR2 (d), and representation in the Fictitious Notch Radius (FNR) finite element model (e).

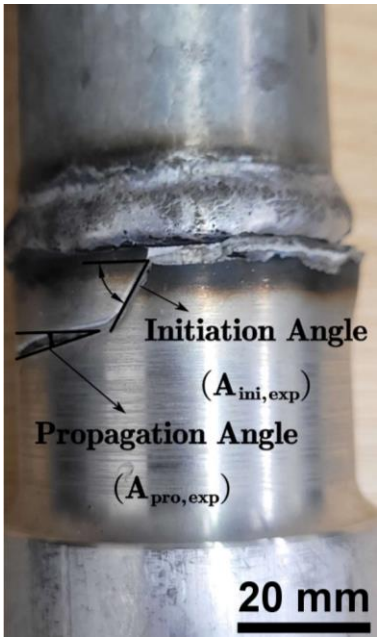

Figure 4. Example illustrating the determination of experimental crack initiation and experimental crack propagation angles under in-phase loading.

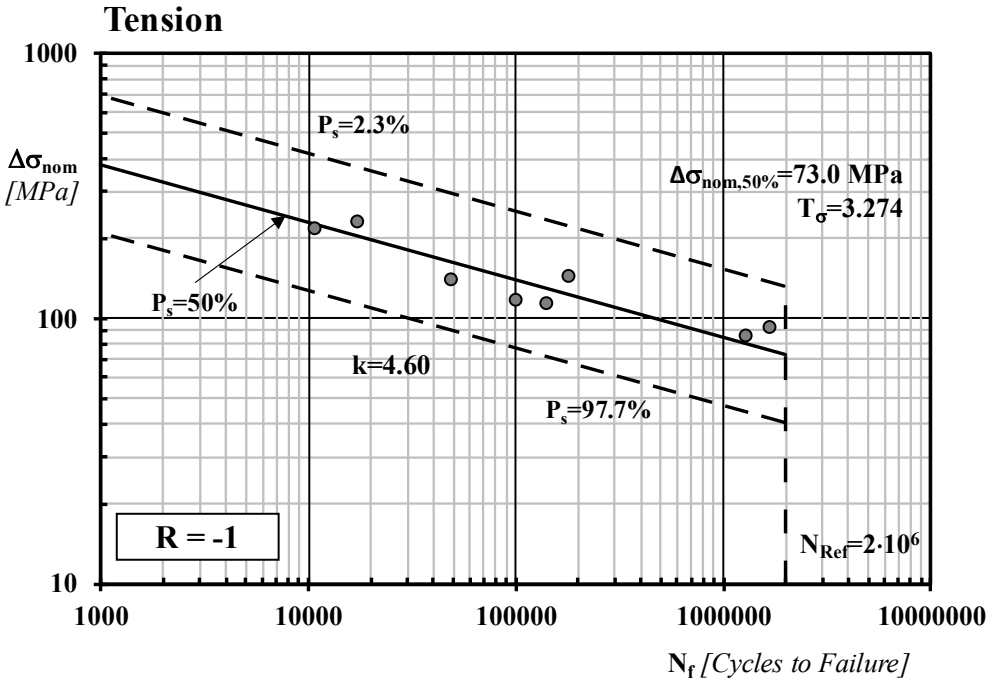
Tension
1000
100
10
Δσnom
[MPa]
Ps=2.3%
Δσnom,50%=73.0 MPa
Tσ=3.274
Ps=50%
k=4.60
Ps=97.7%
R = -1
NRef=2·10⁶
1000
10000
100000
1000000
10000000
Nf [Cycles to Failure]

(a)

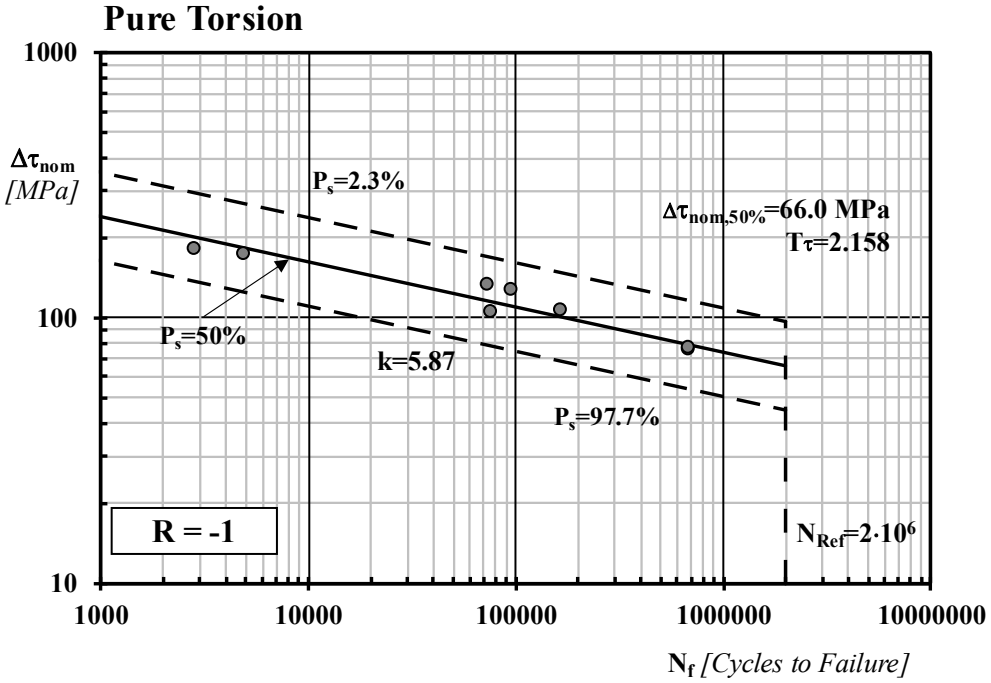
Pure Torsion
1000
100
10
Δτnom
[MPa]
Ps=2.3%
Δτnom,50%=66.0 MPa
Tτ=2.158
Ps=50%
k=5.87
Ps=97.7%
R = -1
NRef=2·10⁶
1000
10000
100000
1000000
10000000
Nf [Cycles to Failure]

(b)

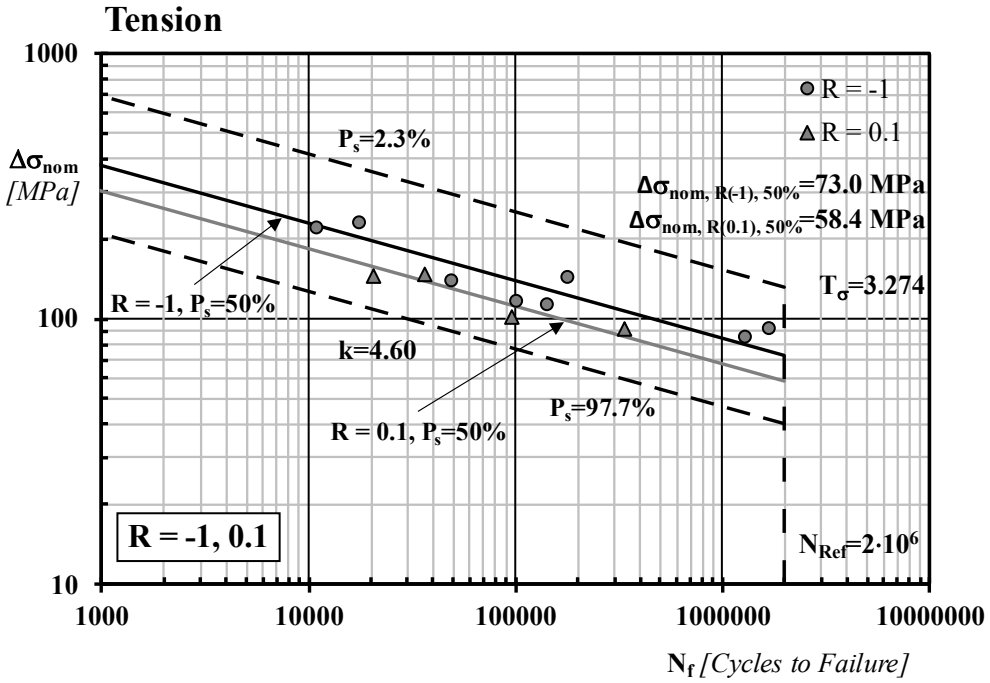

(c) (k factors of one-sided tolerance limit for norm dis)

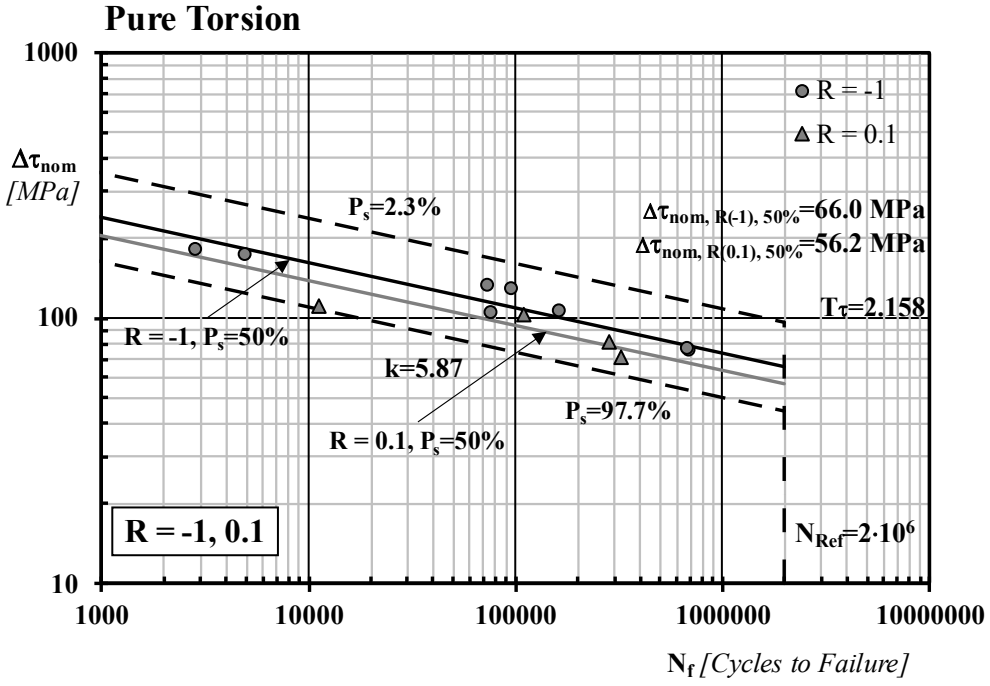

(d)

Figure 5. S–N curves for aluminium-to-steel welded joints under uniaxial (a, c) and pure torsional (b, d) loading. Figures (a) and (b) show regression fits for R=-1 fatigue data; (c) and (d) overlay R = 0.1 results onto the corresponding R = -1 scatter bands using parallel slopes to illustrate mean-stress sensitivity.

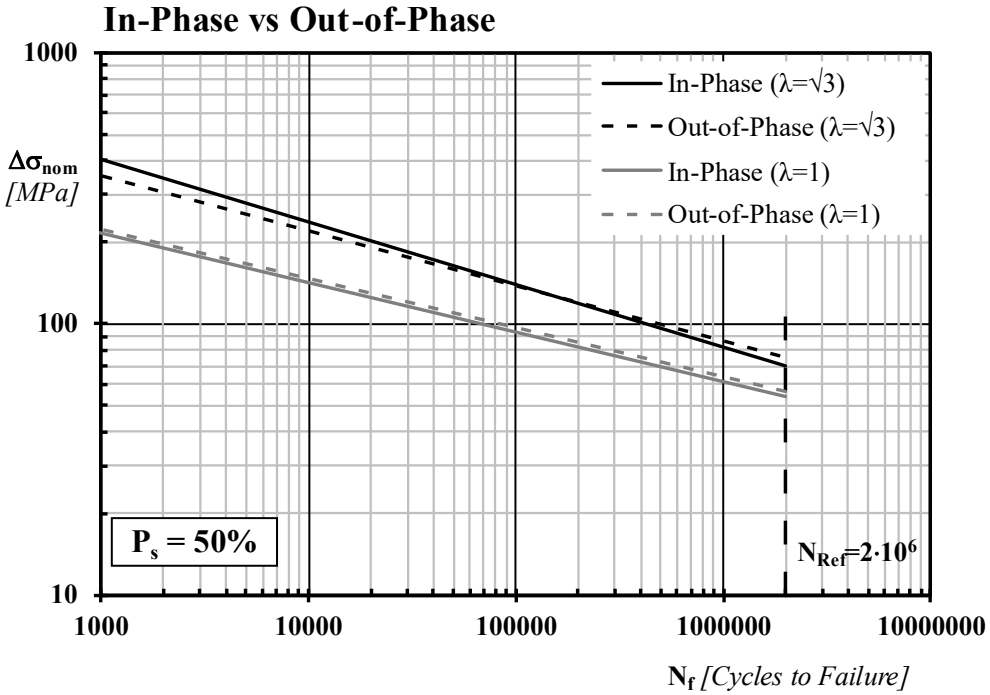

Figure 6. S–N curves under in-phase and out-of-phase fatigue loading at λ=1 and λ=√3, illustrating the influence of loading proportionality on fatigue strength.

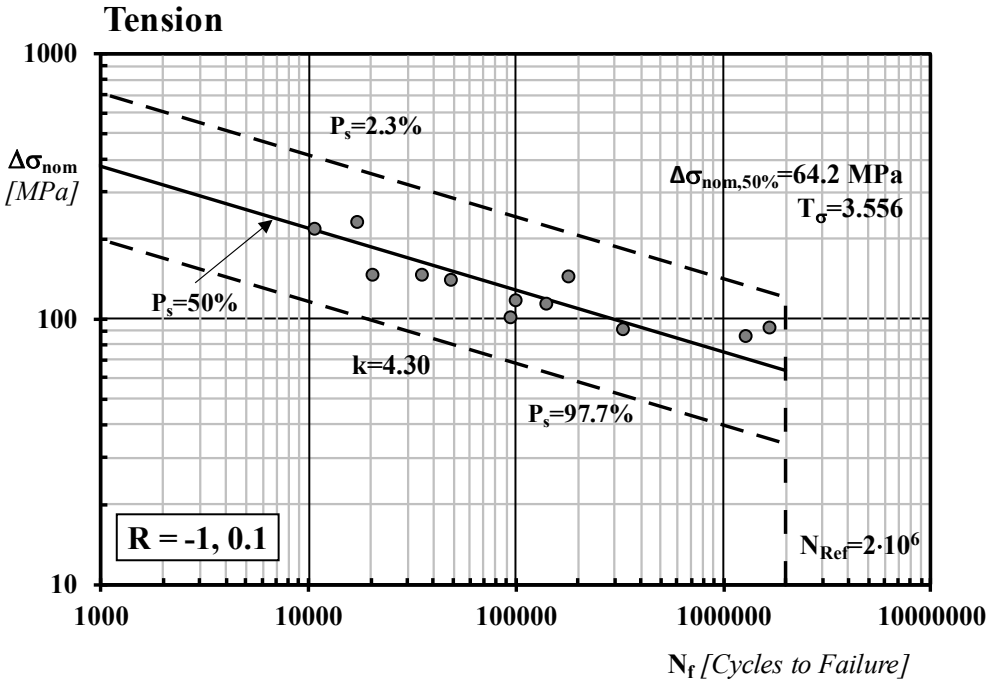
Tension
1000
100
10
Δσnom
[MPa]
Ps=2.3%
Δσnom,50%=64.2 MPa
Tσ=3.556
Ps=50%
k=4.30
Ps=97.7%
R = -1, 0.1
NRef=2·10^6
1000
10000
100000
1000000
10000000
Nf [Cycles to Failure]

(a)

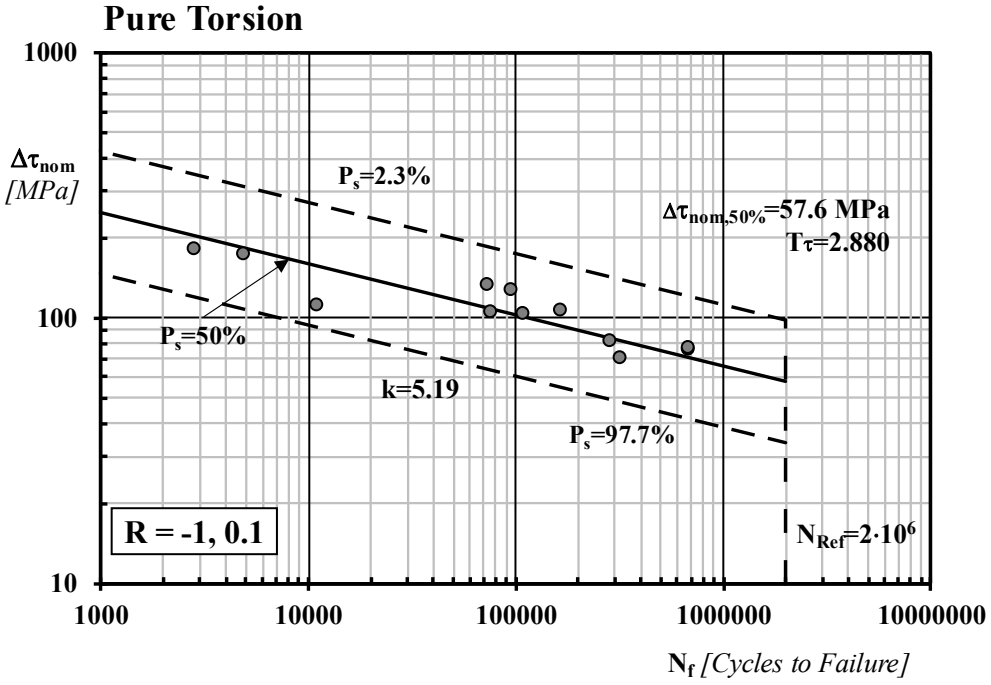
Pure Torsion
1000
100
10
Δτnom
[MPa]
Ps=2.3%
Δτnom,50%=57.6 MPa
Tτ=2.880
Ps=50%
k=5.19
Ps=97.7%
R = -1, 0.1
NRef=2·10^6
1000
10000
100000
1000000
10000000
Nf [Cycles to Failure]

(b)

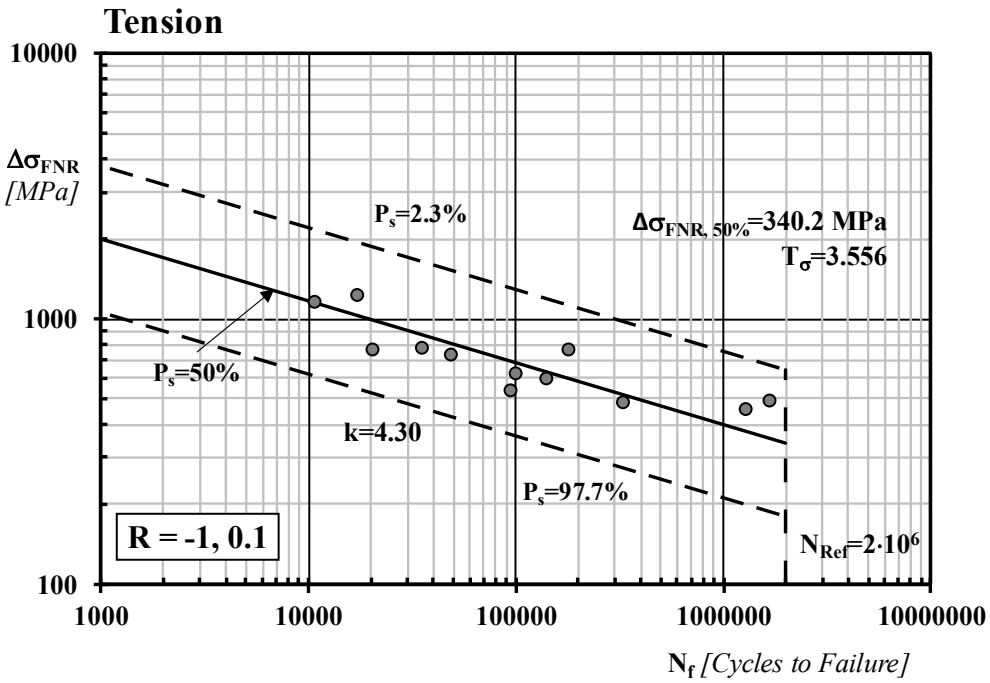

(c)

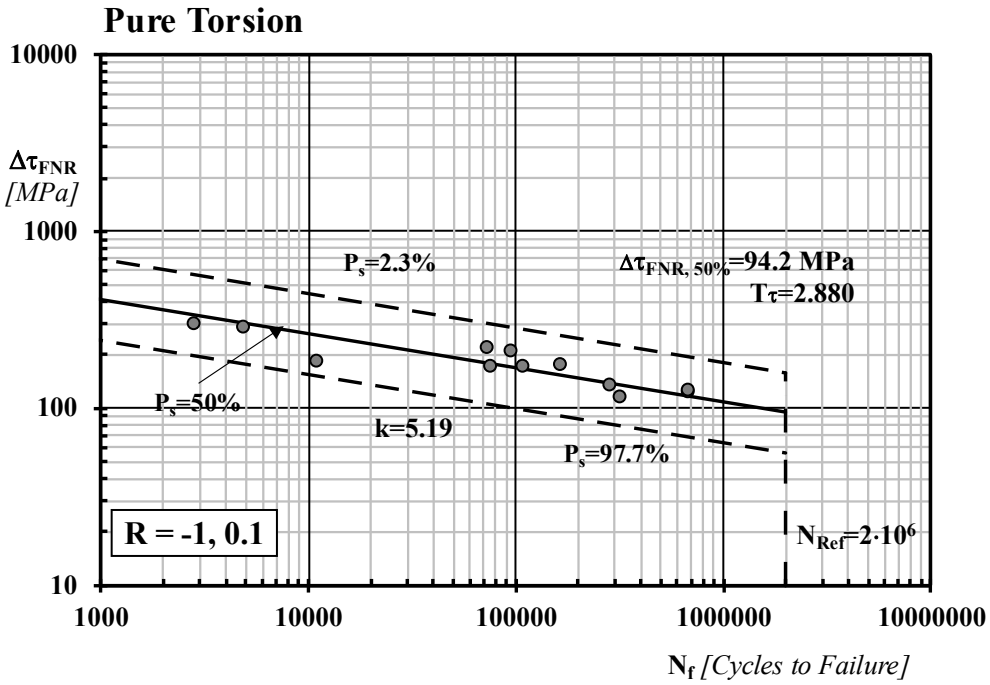

(d)

Figure 7. S–N curves for aluminium-to-steel welded joints under (a) uniaxial and (b) torsional loading using the NS approach, and (c-d) the FNR approach. All plots include R = –1 and R = 0.1 fatigue data within the fitted scatter bands.

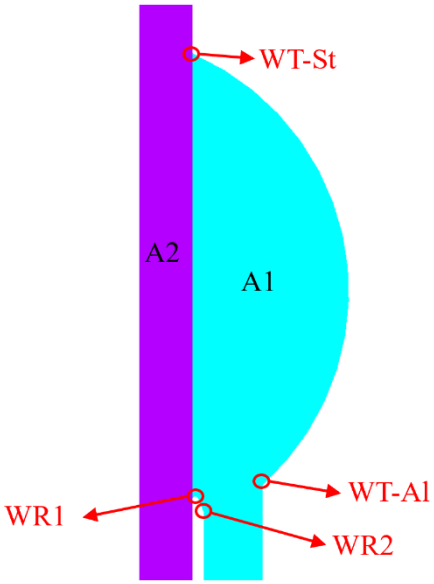

A1: Aluminium (E = 70 GPa, ν = 0.33)
A2: Steel (E = 210 GPa, ν = 0.30)

r_{ref} = 0.05 mm

Critical FNR Sites

SCFs:
K_{ta} = 5.30
K_{tt} = 1.64

Applied Nominal Axial Stress = 1 MPa

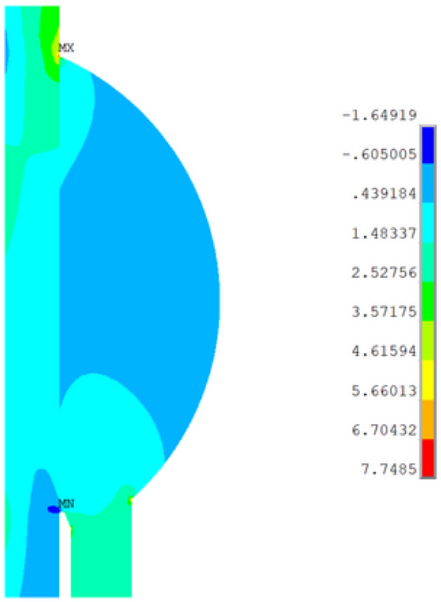

Applied Nominal Torsional Stress = 1 MPa

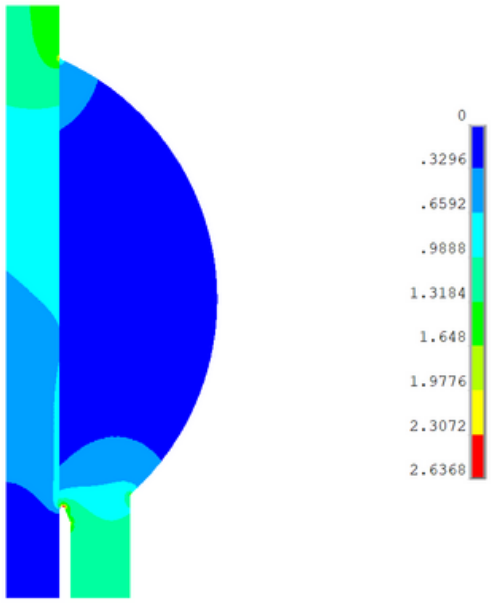

(a)

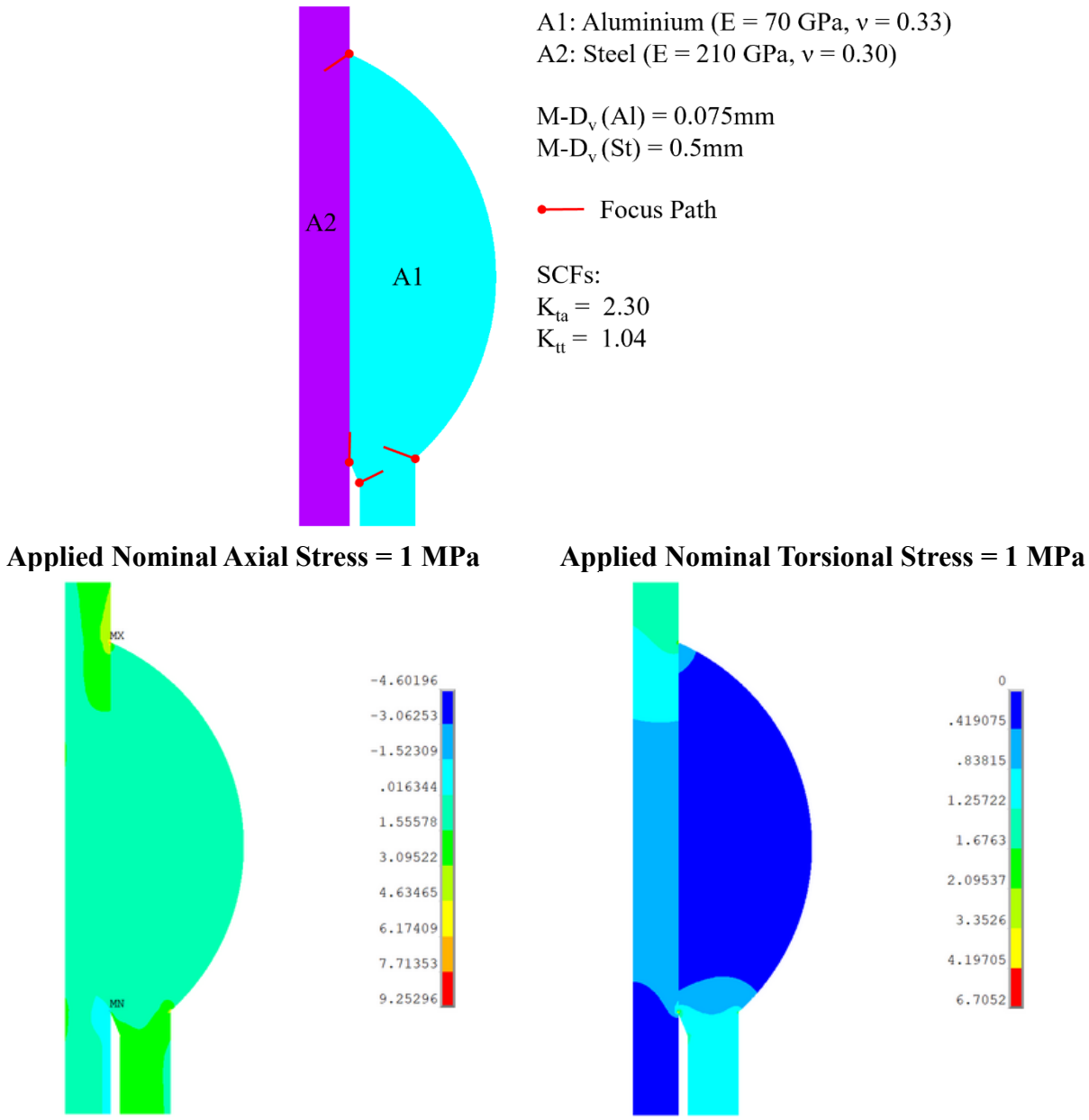

Figure 8. Finite element model of the weld region and representative maximum principal stress contours for (a) FNR and (b) TCD-PM approach, showing critical locations and focus paths from weld toe/root locations used in multiaxial fatigue assessment.

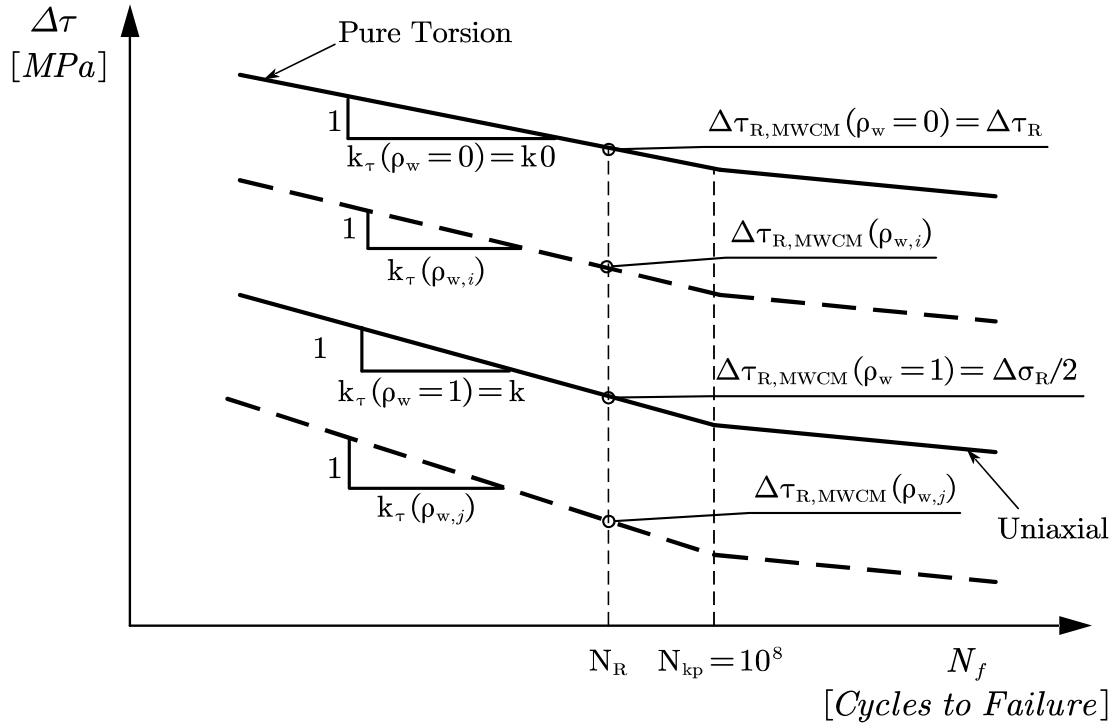

Figure 9. Modified Wöhler diagram used in the MWCM, showing the relationship between shear stress range ($\Delta\tau$), fatigue life (N_f), and the multiaxiality parameter (ρ_w).

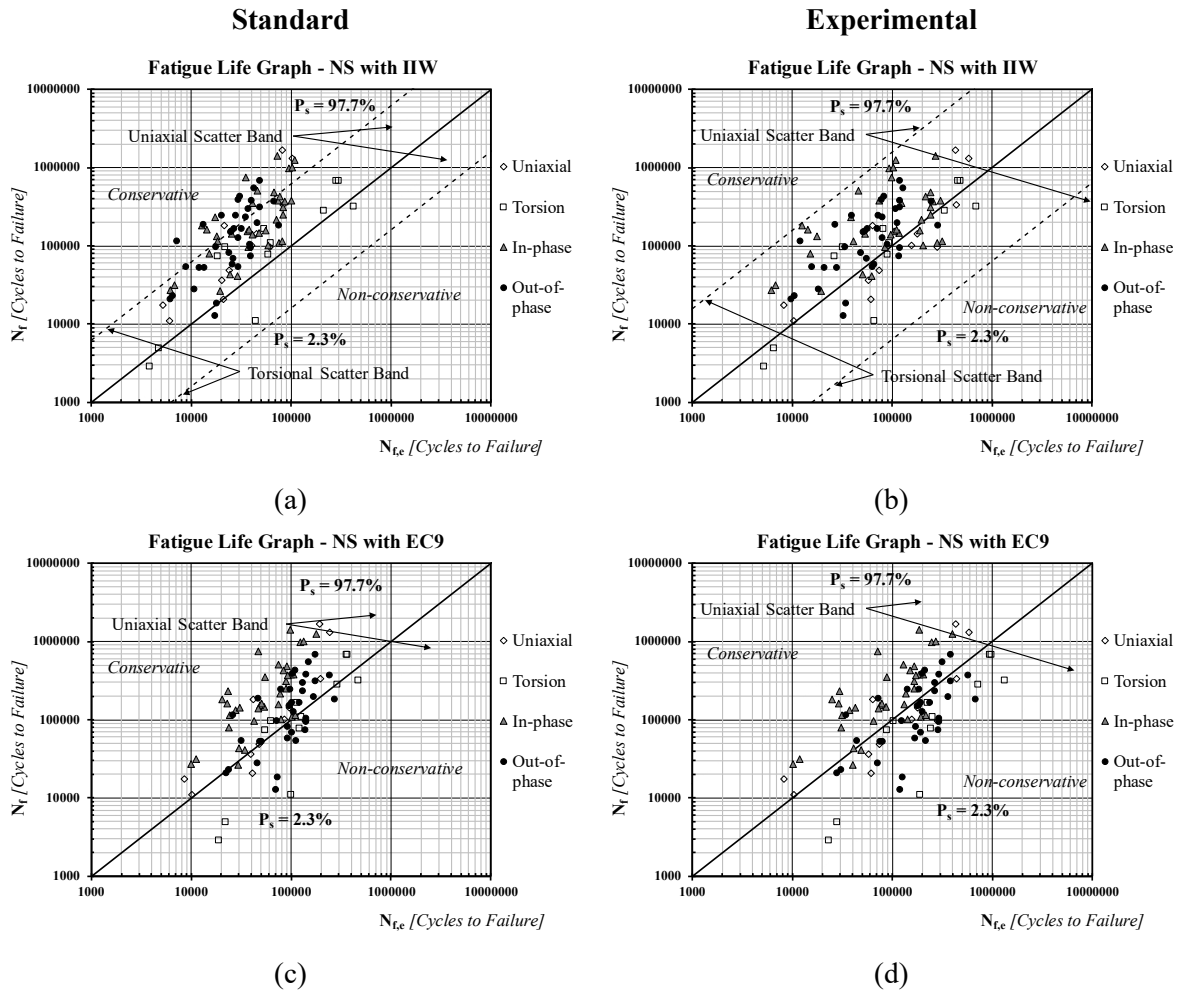

Figure 10. Nominal Stress (NS) approach: fatigue life estimations for as-welded hybrid aluminium-to-steel joints with (a-b) IIW and (c-d) EC9 criteria, comparing standard and experimental reference strengths at P_s=50%.

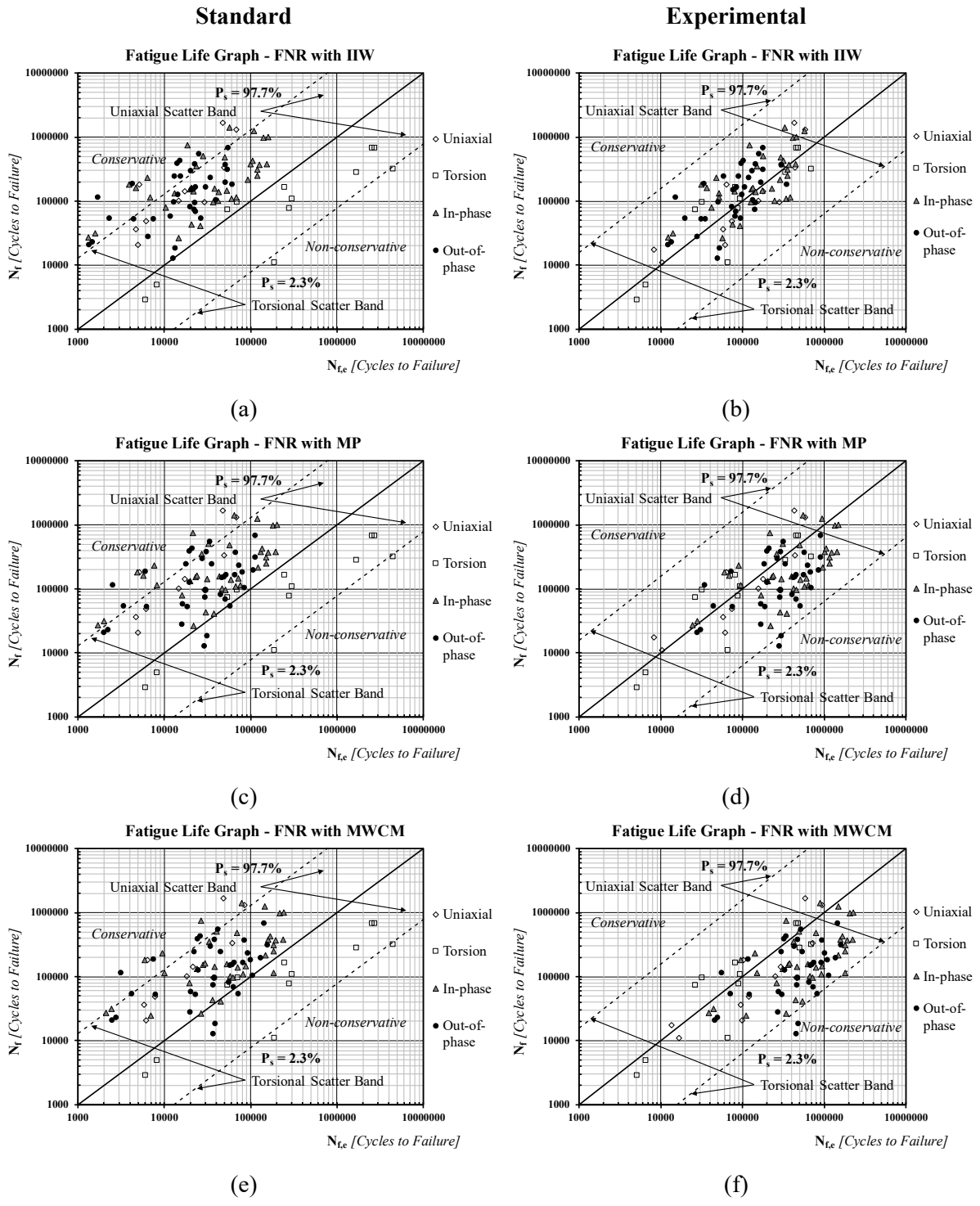

Figure 11. Fictitious Notch Radius (FNR) approach: fatigue life estimations for as-welded hybrid aluminium-to-steel joints with (a-b) IIW, (c-d), and (e-f) MWCM criteria, comparing standard and experimental reference strengths at P_s=50%.

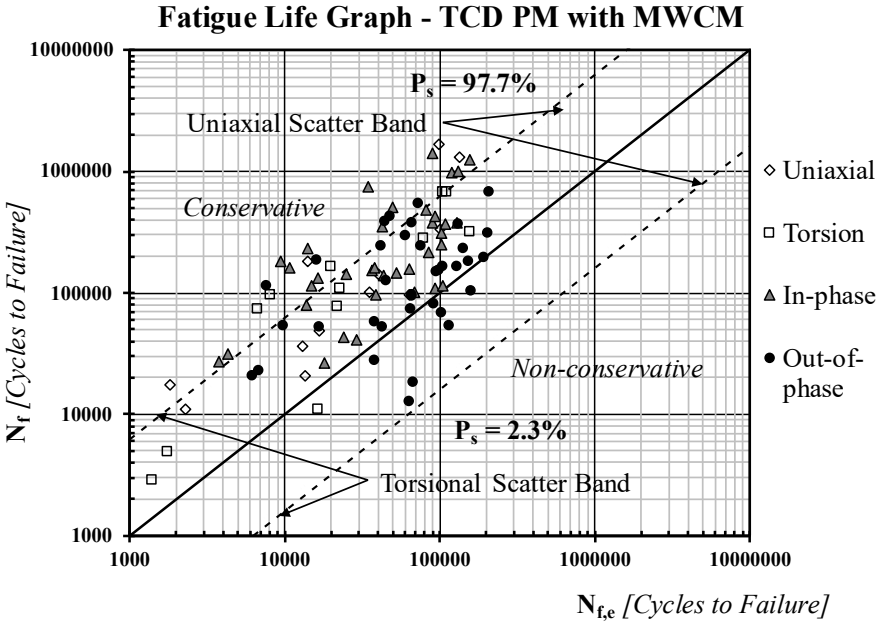

Figure 12. Fatigue life estimations for as-welded hybrid aluminium-to-steel joints using TCD PM approach with the MWCM, based on standard reference strength at P_s=50%.